MASTER'S DEGREE THESIS

Modelling, simulation, and optimization of hot stove operation

Religia Shaliha

Supervisors:
Professor Henrik Saxén
Docent Mikko Helle

Åbo Akademi University
Faculty of Science and Technology
Process and Systems Engineering Laboratory
2020

Abstract

This thesis focuses on modelling and simulation of the operation of a system of three hot stoves used for preheating of the combustion air in the ironmaking blast furnace. A dynamic mathematical model of the stove set was developed for the purpose. Several sample cases were investigated to examine how the hot stoves characteristics, the bypass configuration, and the system operation variables influence the behavior as well as the performance of the entire hot-stove system. In addition, a brief optimization problem has been also studied with the goal to achieve optimum blast temperature.

The model developed in this work considers the heat transfer phenomena throughout the hot stove operation sequence as well as the interconnection between the stoves within the system. In addition, the effects of changes in different operation parameters, i.e., system full-cycle duration, stoves on-blast periods, temperature target of the blast, fuel rate, and enrichment by external fuel, on the overall performance of the system were also studied in the simulations. As the model is programmed with adjustable parameters, it can easily be adapted to any other specific hot-stove system to allow for more accurate and applicable outputs.

Keywords: thermal regenerator, cowper, bypass, checkerwork, pdepe

Acknowledgements

This master's thesis was conducted at Process and Systems Engineering laboratory within Chemical Engineering at the Faculty of Science and Engineering at Åbo Akademi University.

I would like to thank my supervisor Professor Henrik Saxén for the guidance and the insightful discussions we had during the construction of this thesis. I would like to also thank Docent Mikko Helle and M.Sc. Mauricio Roche for all the help related to the computer programming. Many thanks are also addressed to SSAB Raahe for providing financial support as well as reference data for this thesis.

Last but not least, my biggest gratitude goes to my partner and my family for their everlasting support during my journey in this master's program.

Table of contents

List of figures

List of tables

Nomenclature

Latin characters

$A_{\mathrm{c,outer}}$	Outer area of a single channel along checkerwork length [m^2]
$A_{\mathrm{cross,stove}}$	Radial cross section area of a cowper [m^2]
c_{p}	Specific heat capacity [J/kg.K]
D_{h}	Hydraulic diameter of a single channel [m]
E_{error}	Relative percentage of error in the gas-solid energy balance
E_{g}	Energy gained/discharged by the gas [J]
E_{s}	Energy gained/discharged by the solid [J]
h	Heat transfer coefficient [$W/m^2.K$]
h_{blast}	Total heat transfer coefficient during on-blast cycle [$W/m^2.K$]
h_{ca}	Specific enthalpy of combustion air [kJ/kg]
h_{conv}	Convective heat transfer coefficient [$W/m^2.K$]
h_{fuel}	Specific enthalpy of fuel [kJ/kg]
H_{fuel}	Heating value of fuel [kJ/kg]
h_{cg}	Specific enthalpy of combustion gas [kJ/kg]
h_{heat}	Total heat transfer coefficient during on-gas cycle [$W/m^2.K$]
h_{rad}	Radiative heat transfer coefficient [$W/m^2.K$]
k	Thermal conductivity [W/m.K]
$\mathcal{K}_{\mathrm{qss}}$	Set of time steps in a hot stove cycle in quasi-steady state operation
L	Checkerwork height [m]
M	Molecular weight [mol/kg]
$\dot{m}_{\mathrm{bl,in}}$	Mass flowrate of blast flowing into checkerwork [kg/s]
$\dot{m}_{\mathrm{bl,tot}}$	Total mass flowrate of blast (before flow diversion) [kg/s]
$\dot{m}_{\mathrm{cg}}$	Mass flowrate of combustion gas [kg/s]
$\dot{m}_{\mathrm{g,in}}$	Mass flowrate of gas flowing into checkerwork [kg/s]
$\dot{n}$	Molar flowrate [mol/s]
N	Uppermost segment of discretized checkerwork
N_{brick}	Number of bricks
$N_{\mathrm{c,brick}}$	Number of channels in a brick
$N_{\mathrm{c,check}}$	Number of channels in checkerwork
$N_{\mathrm{step\ z}}$	Number of spatial steps across the discretized checkerwork height
Nu	Nusselt number
P	Pressure [Pa]
Pr	Prandtl number
$\bar{Q}_{\mathrm{loss}}$	Average rate of heat loss [W]
$\dot{Q}_{\mathrm{rad}}$	Rate of heat radiation [W]
r	Radius of gas channel [m]
R	Ideal gas constant [J/mol.K]
Re	Reynolds number
r_i	Channel inner radius [m]
r_o	Channel outer [m]
t	Time [s]
T	Temperature [K]

$T_{\text{air,in}}$	Purging air temperature at stove inlet [°C]
$t_{\text{blast},i}$	On-blast period for stove i [s]
$T_{\text{bl,end}}$	Final blast temperature after "mixing" of flows [°C]
$T_{\text{bl,in}}$	Blast temperature at stove inlet [°C]
$T_{\text{bl,out}}$	Blast temperature at stove outlet [°C]
$T_{\text{bl,tr}}$	Blast temperature target after "mixing" of flows [°C]
$T_{\text{c,max}}$	Maximum temperature at checkerwork cold end [°C]
$T_{\text{cg,in}}$	Combustion gas temperature at stove inlet [°C]
t_{cyc}	Full cycle length of the hot stove system [s]
$T_{\text{h,max}}$	Maximum temperature at checkerwork hot end [°C]
$t_{\text{heat},i}$	On-gas period for stove i [s]
$t_{\text{purge},i}$	Purging duration for stove i [s]
$t_{\text{switch tot},i}$	Total switching durations for stove i [s]
$\dot{V}$	Volumetric flowrate [m^3n/s]
V_{brick}	Volume of a single brick [m^3]
W_{brick}	Width of a single brick [m]
$x_{\text{check,stove}}$	Share of radial cross section area of checkerwork in a cowper
$x_{\text{bl,in}}$	Flow share of the blast flowing into checkerwork
x	Component mass fraction in a mixture
y	Component molar fraction in a mixture
z	Spatial position [m]
Z_{brick}	Height of a single brick [m]
Z_{check}	Height of checkerwork [m]

Greek characters

α	Absorptivity
ϵ	Emissivity
ϕ	Interaction parameter between two species
λ	Air excess factor
μ	Viscosity [Pa.s]
ρ	Density [kg/m^3]
σ	Stefan-Boltzmann constant ($5.67 \cdot 10^{-8}$) [$W/m^2.K^4$]
υ	Flow velocity [m/s]

Subscript

g	Gas
in	Input (at boundary)
m	Mixture
out	Output (at boundary)
s	Solid
w	Solid wall/surface

Superscript

max	Maximum value
min	Minimum value

1 Introduction

1.1 Background

The iron- and steel-making industry is one of the most energy- and carbon-intensive sectors which accounts for 20% of the total energy use in the manufacturing industries [1]. Due to its high reliance on fossil fuels as both energy carrier and reducing agent, the iron and steel industry is the largest CO_2 emitter in the industrial sector and accounts for 4-7% of the global emissions and a similar range in Europe [2]. Because of this, energy-saving efforts are very important in order to progress towards a more efficient and green development of the iron- and steel-making processes.

One of the possible opportunities to reduce the energy consumption in the iron- and steel-making process is through the optimization of the hot stove operation. Hot stoves, or cowpers, are regenerative heat exchangers which serve the function of providing a constant flow of hot combustion air ("blast") for the blast furnace in the ironmaking process. Commonly, there are three to four hot stoves operating in a system providing hot blast for one blast furnace. The operation of the hot-stove system is highly dynamic as it involves two alternating main phases during the operation of each stove, namely a heating phase and a cooling phase. Furthermore, because of the highly interconnected characteristics of the blast preheating system, both operation parameters and performance of each stove influence the other stoves in the set.

High blast temperature is one of the essential technical characteristics to be achieved in the operation of a blast furnace. Elevating blast temperature can promote an improvement of performance of the overall iron ore reduction process in the blast furnace (i.e., increase productivity), and decrease the consumption of coke and fuel as well as minimize the CO_2 emission [3]. According to a general practice, an increase of 10 °C in the hot blast temperature corresponds to coke consumption reduction by 1 kg/t hot metal [4].

To be able to improve the performance of a hot-stove system, a good understanding of its operational behavior is necessary. Mathematical models of hot stoves have been presented since the 1960s. The model by Wilmott in 1968 [5] included the variation of gas flow rate and gas properties, while Razelos and Benjamin in 1977 [6] also considered the temperature-dependent properties of the checkerwork. The investigation by Kwakernaak et al. in 1970 [7] focused on determining the optimum thermal efficiency of a hot stove in a staggered parallel system by adopting a numerical calculation using the trapezoidal discretization method. In 2000, Muske et al. [8,9] developed a model-based control of a hot stove where the dynamic heat transfer with temperature dependent gas and solid properties were considered. While most of the earlier studies considered only a single stove, the more recent work by Zetterholm in 2017 [1] developed a model for multiple hot stoves in the entire stove system. However, further insight about the influence of different performance of each stove in the system is needed as well as a deeper understanding of the bypass configuration.

1.2 Objective

The main objective of this work is to build a model that simulates the operational behavior of a system of three serial hot stoves with different efficiencies based on the fundamental heat transfer equations. This model is further to be used as a tool to investigate some operation strategies to achieve optimum hot stoves performance with higher blast temperature and/or minimum consumption of coke and other external fuel in the blast furnace.

2 Process Description

2.1 Overview of the Blast Furnace Ironmaking Process

The blast furnace ironmaking process is currently the most common route of pig iron production worldwide. In a blast furnace, heat and mass transfer and chemical reactions occur at high temperatures in a counter current flow configuration. The main input of this process consists of iron ore (pellets, sinter or lump ore) as the main raw material, limestone, and coke as well as coal. Limestone is added to remove unwanted components such as sulfur, silica, alumina, and magnesia, from the iron ore, whereas coke and coal serve as the reducing agent and as the energy carriers in the blast furnace process. In addition, coke also acts as a support structure for the layers of materials in the blast furnace and as a bed through which the molten materials trickle down the blast furnace and the gas from the reduction process flows upwards.

At the top of the blast furnace, iron ore, coke, and limestone are charged in layers. Meanwhile, hot air and an additional reducing agent, such as pulverized coal, natural gas or fuel oil, are introduced through the tuyeres at the bottom part of the blast furnace. As the burden sinks in the blast furnace, it travels through a series of different temperature zones, at which different thermochemical conversions take place. A schematic of a blast furnace is depicted in Figure 2.1 [10].

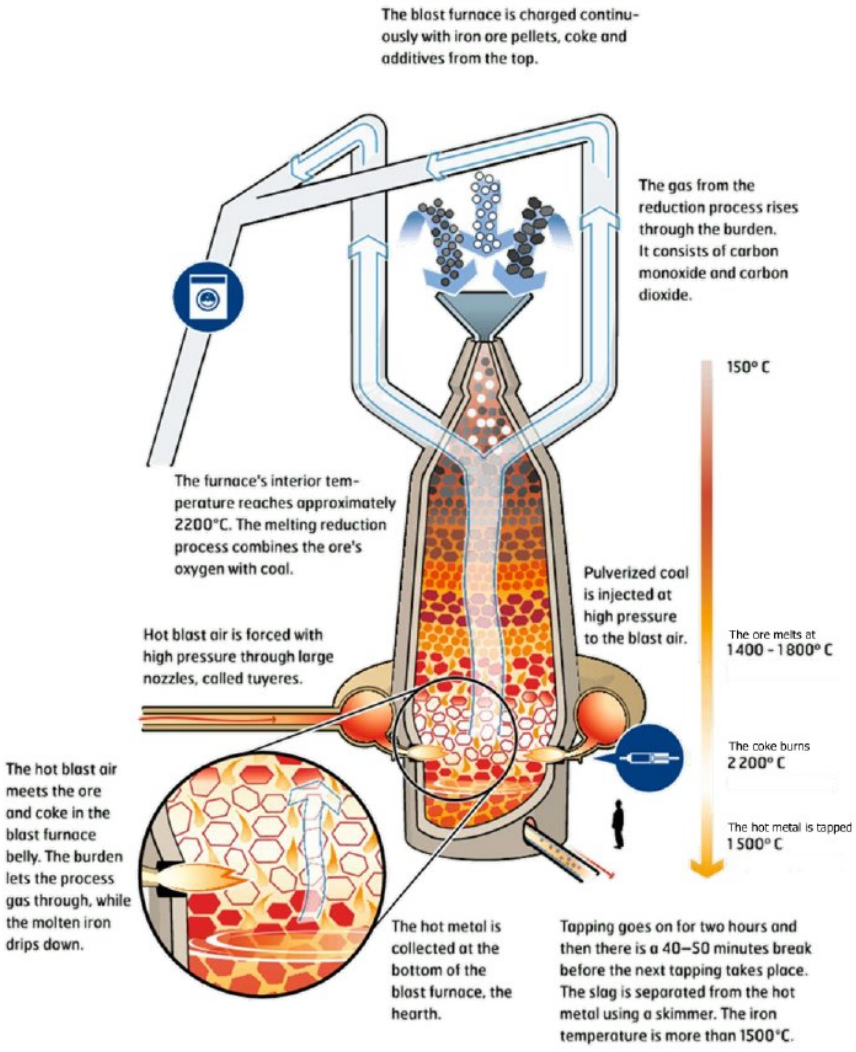

Figure 2.1 Schematic figure of a blast furnace [10]

A series of chemical reactions occur during the reduction process in the blast furnace according to the local temperature as well as the state of the feed and the gas. During the process in the blast furnace, iron ore is heated up from ambient temperature to 1400 - 1450 °C. The main reducing component for the overall process is the CO, which is formed from the oxidation of the coal and coke in the lower region of the blast furnace.

$$C + O_2 \rightarrow CO_2$$

CO is also regenerated by the Boudouard (or "solution-loss") reaction

$$C + CO_2 \leftrightarrow 2\ CO$$

At 500 - 900 °C, hematite (Fe_2O_3) in the iron ore is reduced to magnetite (Fe_3O_4). In addition, the reduction of magnetite to wüstite (FeO) takes place at a similar temperature range.

$$3\ Fe_2O_3 + CO \leftrightarrow 2\ Fe_3O_4 + CO_2$$

$$Fe_3O_4 + CO \leftrightarrow 3\ FeO + CO_2$$

In the lower region of the blast furnace, where the temperature gradually rises to 1400 °C, wüstite is further reduced to iron through both indirect and direct reduction.

$$FeO + CO \leftrightarrow Fe + CO_2$$

$$FeO + C \leftrightarrow Fe + CO$$

In this region the iron and slag phases also melt and separate. It should be stressed that also hydrogen acts as a reducing agent participating in similar reactions as those outlined for CO above (where CO and CO_2 can be replaced by H_2 and H_2O, respectively). The resulting outputs of the blast furnace are molten pig iron, slag, and blast furnace gas. Due to its higher density, the molten pig iron is naturally separated from the unwanted impurities bound in the slag and is tapped at the bottom of the blast furnace. Meanwhile, the blast furnace gas is extracted at the top of the furnace. As this gas has some heating value due to its CO and H_2 content, which typically are around 20% and 3%, it can be utilized to provide energy required in other sections of the steel plant. One of the typical uses of the blast furnace top gas is to fuel the hot blast stoves during the heating phase.

2.2 Hot Blast Stoves

Hot blast stoves are an essential auxiliary equipment to blast furnace operation which provides a constant flow of hot blast for the blast furnace process. Hot blast stoves are tall, cylindrical thermal regenerators which consist of three main parts referred to as the combustion chamber, the dome, and the checkerwork or the brick zone. This equipment is constructed of refractory materials that are capable of withstanding elevated temperature as well as storing thermal energy. A schematic view of a typical hot blast stove is shown in Figure 2.2.

Throughout its operation, a hot stove goes through alternating cycles of heating (on-gas) and cooling (on-blast), with switching/idle period in between. During the heating phase, blast furnace top gas is combusted inside the combustion chamber. It is also possible to apply fuel enrichment by adding a fraction of other external fuel, such as coke oven gas, natural gas, or LPG to raise the combustion temperature. The resulting combustion gas that can reach temperatures up to 1300 °C flows by the dome, passes through the channels in the checkerwork, and heats up the bricks in the checkerwork. In contrast, during the cooling phase, pressurized air, which is referred to as cold blast, flows through the hot stove in a reversed direction. This cold blast enters the bottom part of the checkerwork at around 150 °C (which is the temperature reached after compression) and picks up thermal energy as it passes

through the checkerwork. The blast flows through the dome and a part of the combustion chamber and exits the hot stove at over 1000 °C.

The temperature of the hot blast coming out of the hot stove naturally decreases during the cooling phase due to the depletion of the thermal energy stored in the stove. Because of this, the temperature of the hot blast from the hot stoves in some systems is regulated by bypassing a fraction of the cold blast to mix directly with the heated air coming out from the stove. This enables the blast furnace to be supplied with hot blast of constant flow and temperature regardless of the blast temperature drops at the hot stove outlet, which makes it easier to control the thermal level of the blast furnace. However, it comes at the expense of a lower average blast temperature. Therefore, it is usually a rule that the constant blast temperature from the stove set should be kept as high as possible, considering the prevailing conditions.

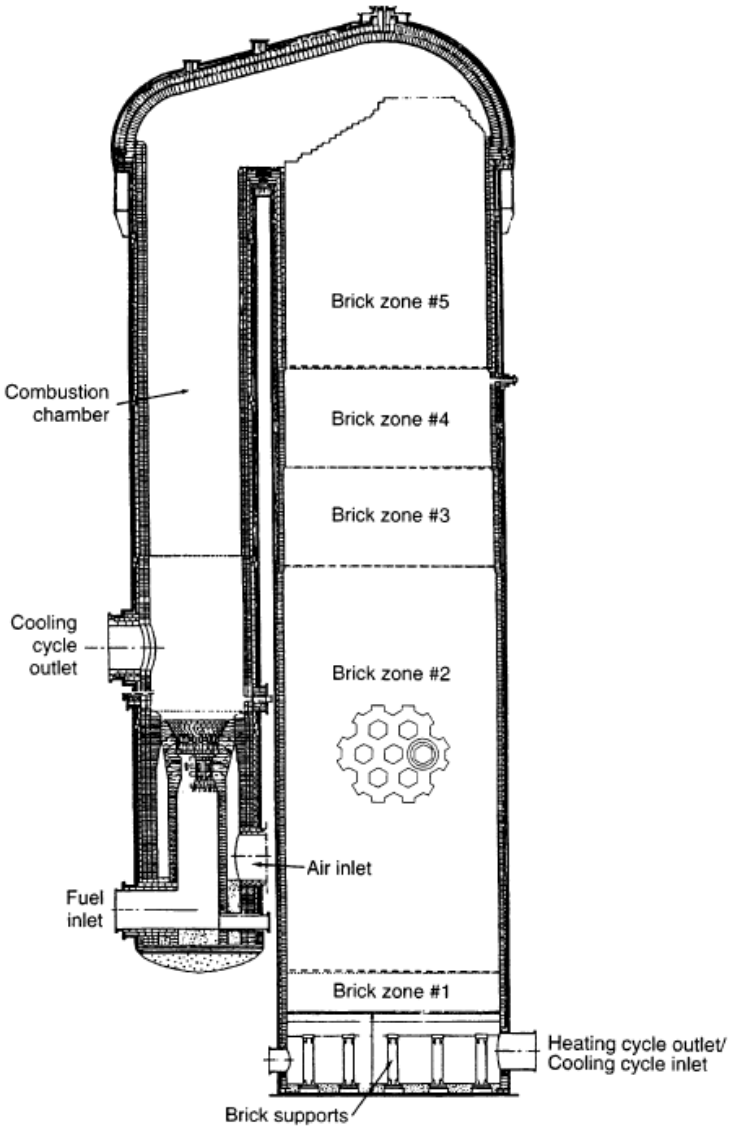

Figure 2.2 Schematic figure of a typical hot stove (with external combustion chamber) [8]

Typically, there are three to four hot blast stoves in operation for a blast furnace. Figure 2.3 depicts a flow schematic of a system with three hot stoves in a bypass main serial configuration connected to a blast furnace. In this kind of arrangement, usually one hot stove is operating in on-blast mode and supplies hot blast for the blast furnace for a certain time period, while the other two stoves in the system are being heated. The on-blast period is normally set such that the hot stove in the on-blast mode can complete the entire on-blast period whilst sustaining the outgoing blast temperature to be higher than the desired level. Once the hot stove in the on-blast mode completes its on-blast period, it is switched into on-gas phase, and another stove in the system takes the turn to supply the hot blast to the blast furnace.

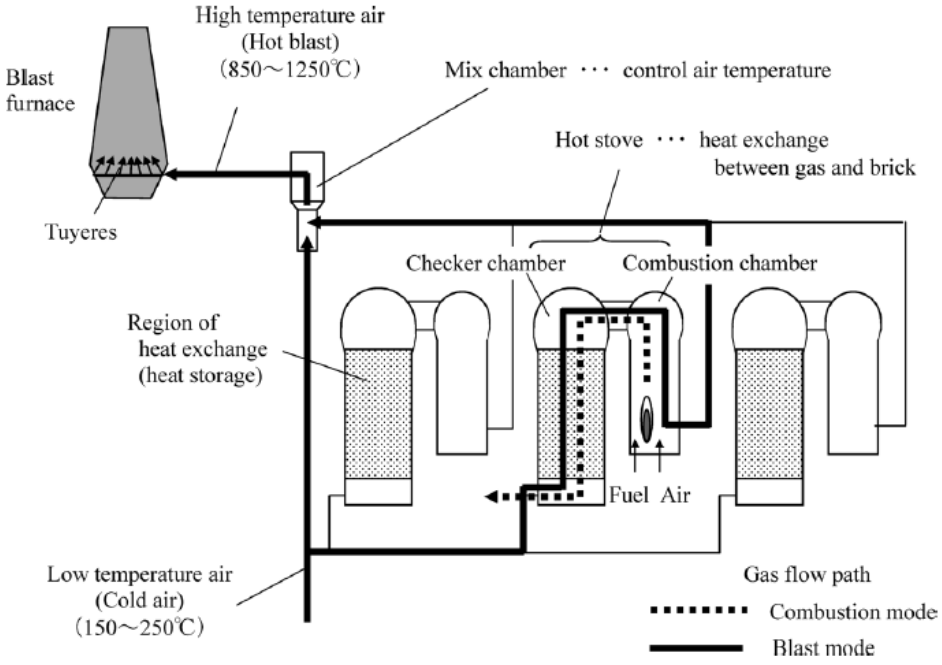

Figure 2.3 Flow schematic of a system of three hot stoves in a bypass main serial configuration connected to a blast furnace [11]

Between the heating and the cooling phase there is a change-over period where a hot stove switches its operation mode. This period includes the required time to regulate the valves that allow the flows of the gas and the air into the hot stove, purge the flue gas and pressurize the hot stove when switching from heating to cooling mode, and to release the high pressure when the hot stove switches from cooling mode to heating mode. Figure 2.4 briefly describes a typical operation sequence of one full cycle in a system of three hot stoves.

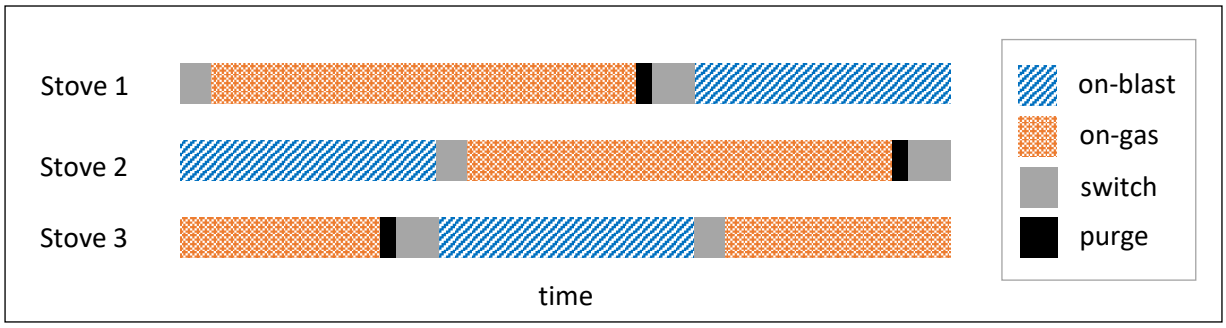

Figure 2.4 Typical operation sequence of one full cycle in a system of three hot stoves [12]

Due to the large size and the dynamics of the valves, the blast flow cannot be switched abruptly. Therefore, there are flow transitions in the beginning and at the end of an on-blast period. In a system without bypass, the blast flow rate ramps up from no-flow when a stove starts the on-blast stage, and ramps down from full-flow to no-flow when a stove finishes the on-blast phase. Meanwhile, during the transitions in a system with bypass, the blast flow distribution looks somewhat different with the presence of the bypass air. Figure 2.5 and Figure 2.6 respectively illustrates the ideal blast flow distribution throughout the cycles in a hot-stove system without bypass and with bypass. Note that the unit of the abscissa is arbitrary. In reality, the flow progresses of the blast and the bypass are not necessarily linear, depending on the characteristics and the dynamics of the valves in the system.

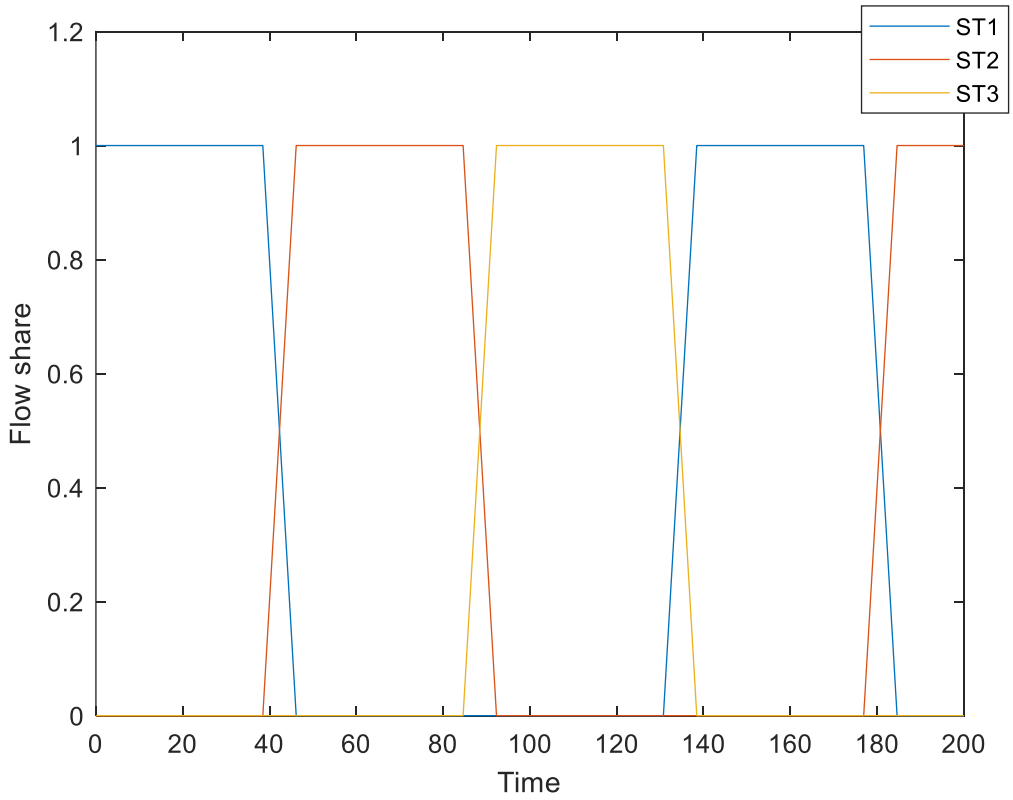

Figure 2.5 Flow distribution of blast in hot-stove system without bypass

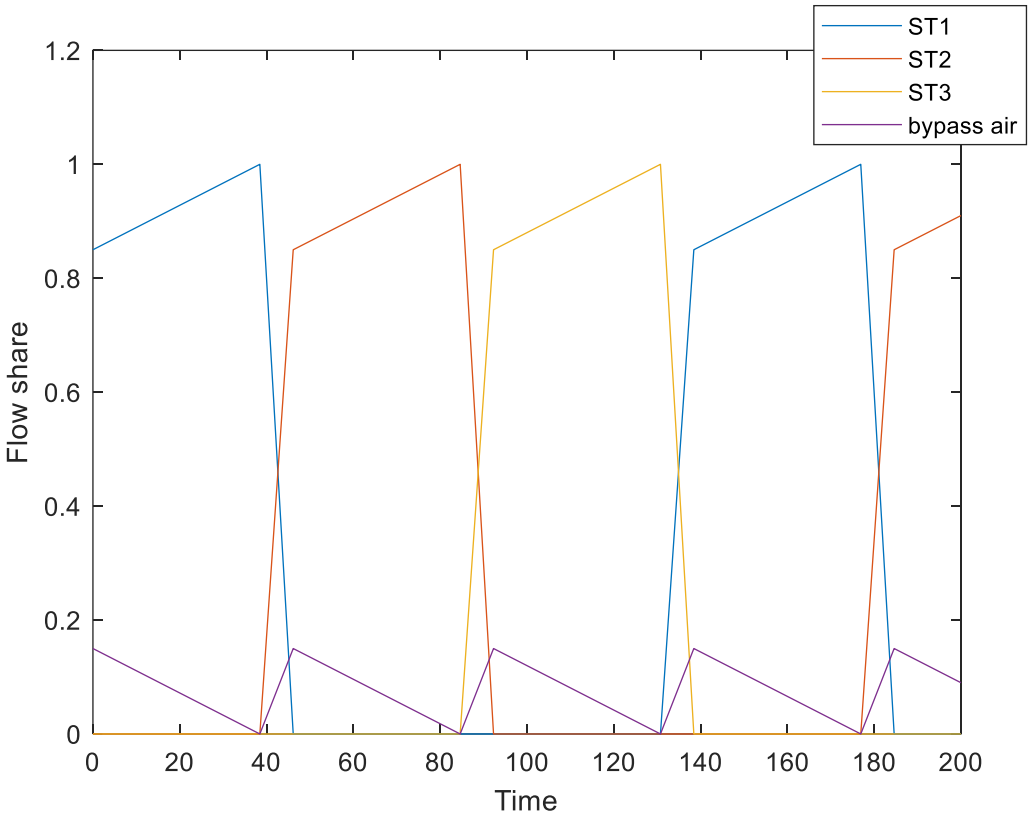

Figure 2.6 Flow distribution of blast and bypass air in a bypass main system

3 Methodology – Modelling and Simulation

3.1 Thermal Regenerator Model

This section describes the way in which the solid material has been approximated in the mathematical model of the stove system.

3.1.1 Refractory Brick/Checker

The checkerwork is constructed of stacked refractory bricks made of fireclay or high alumina material, depending on the zone. These refractory bricks, referred to as checkers, are hexagonal bricks with several channels for gas to pass through. Typically, each checker has 12 equivalent channels. In addition, the top diameter of the gas channel is usually designed to be slightly narrower than the bottom to enhance heat transfer in the stove [8]. The tongue and groove structure at the top and the bottom of the bricks allow them to interlock and to be arranged in the checkerwork compactly. Figure 3.1 shows a schematic of a checker that is being modelled in this work.

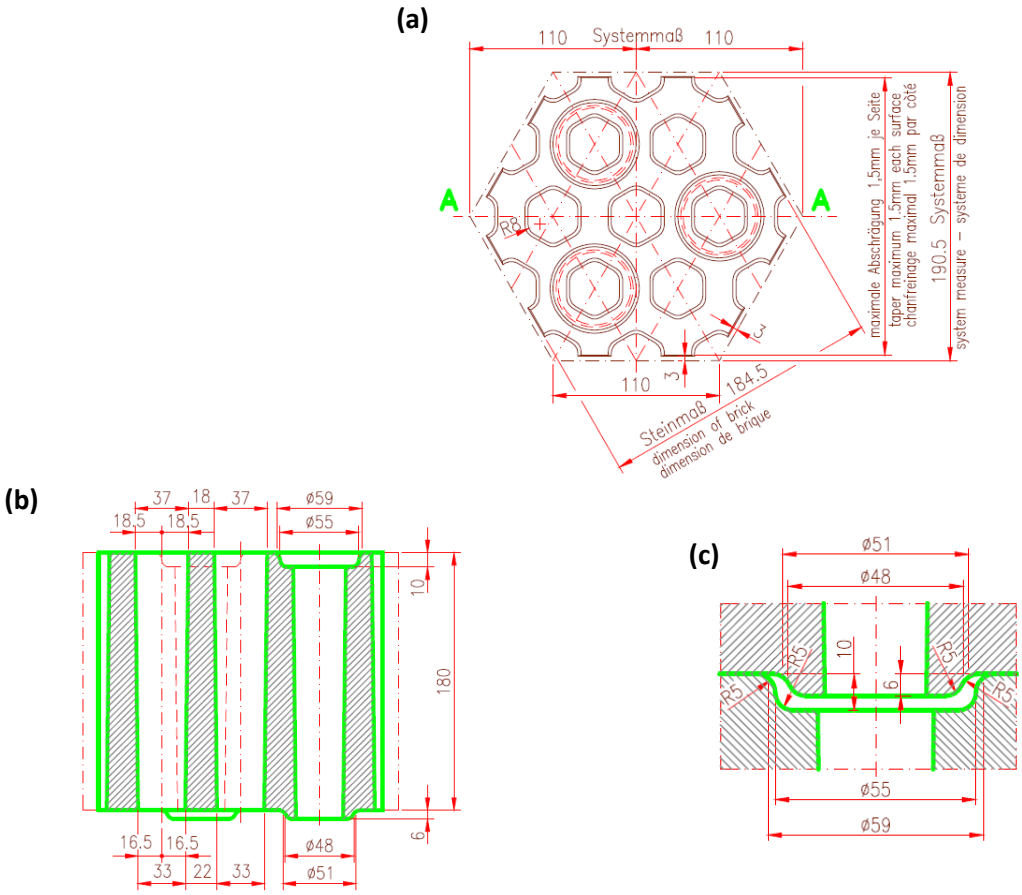

Figure 3.1 Schematic of a checker at SSAB Raahe; (a) top view, (b) axial cross section, (c) tongue and groove structure [13]

3.1.2 Checkerwork Geometry

In this study, hot stoves with internal combustion chambers are considered. Nevertheless, the scope of heat transfer study in this work is limited to only the checkerwork part. The checkerwork region consists of a number of brick courses and it is assumed that each course has uniform number of bricks. The checkerwork part occupies approximately 75% of the total cross section area of the stove. An axial and

radial cross section view of a hot stove at SSAB Raahe is depicted in Figure 3.2 and Figure 3.3 respectively.

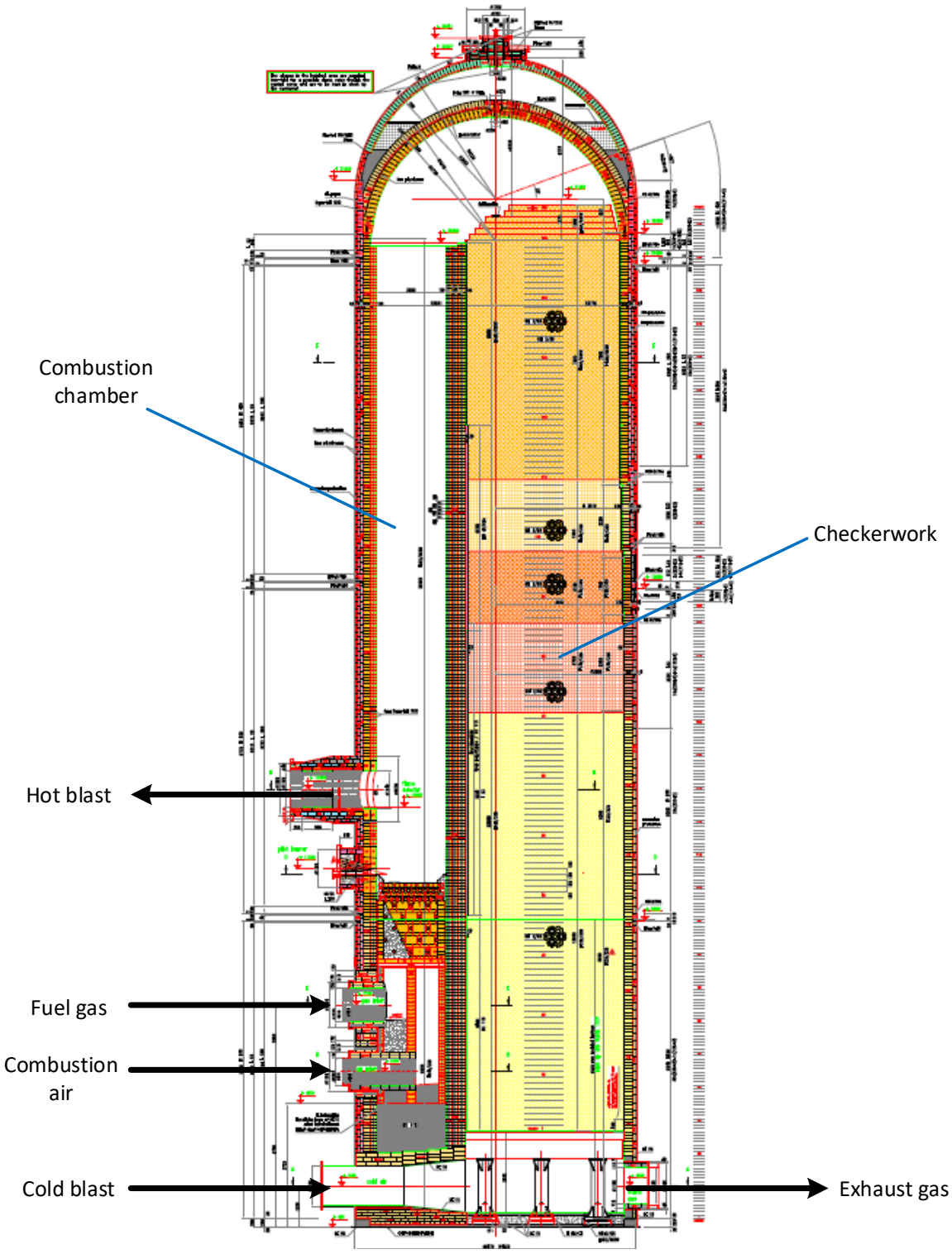

Figure 3.2 Schematic of axial cross section of a hot stove at SSAB Raahe [13]

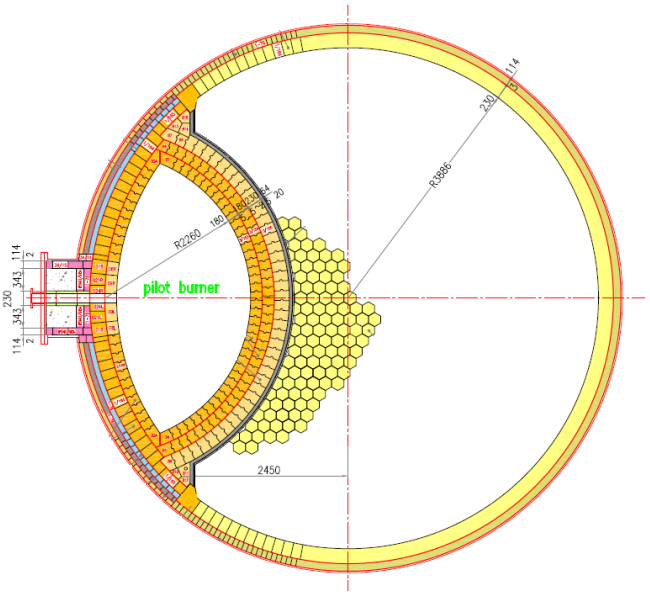

Figure 3.3 Schematic of radial cross section of a hot stove at SSAB Raahe [13]

3.1.3 Approximated Checkerwork Geometry

For simplification, the gas flow distribution through the channels in the checkerwork was assumed to be uniform, hence the calculation in this model was performed only for a single channel. The hexagonal channel was modelled as a circular thick-walled tube with an even inner radius, r_{i}. The outer radius of the circular tube, r_{o}, was determined as described in Equation (1), where V_{brick} is the volume of brick corresponding to 12 channels. In this equation, r_{o} was calculated such that the heat storing capacity of the brick is conserved; thus $r_{\mathrm{o}} - r_{\mathrm{i}}$ can be interpreted as an equivalent wall thickness. Figure 3.4 illustrates a schematic of the modelled geometry of the thermal regenerator and Table 3.1 presents the dimension of the modelled thermal regenerator which is used in the calculations.

$$r_{\mathrm{o}} = \sqrt{r_{\mathrm{i}}^2 + \frac{V_{\mathrm{brick}}}{12\pi Z_{\mathrm{brick}}}} \tag{1}$$

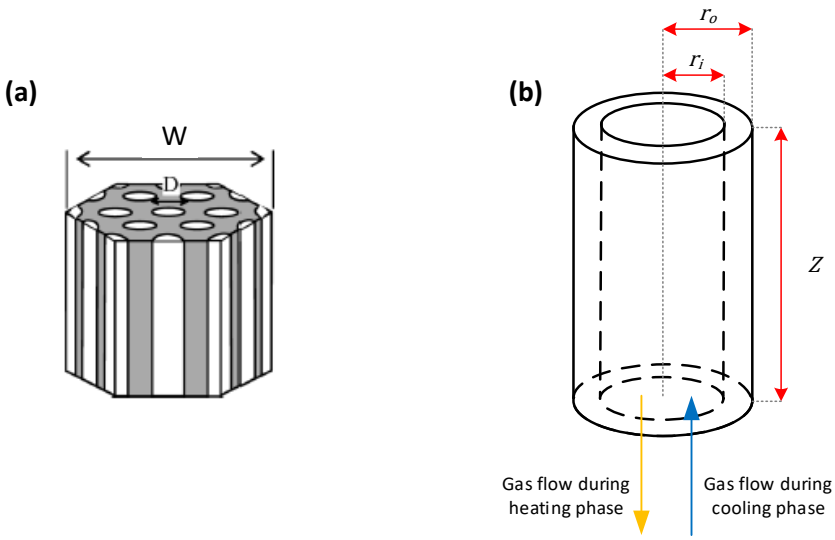

Figure 3.4 Geometry of the modelled thermal regenerator: (a) schematic of a checker [11]; W denotes the (largest) width of the brick and D denotes the hydraulic diameter of the gas channels, (b) modelled gas channel

Table 3.1 Dimension data of the modelled thermal regenerator

Parameter	Value	Unit
Z_{brick}	180	mm
W_{brick}	220	mm
D_{h}	35	mm
V_{brick}	3.28	dm^3
Equivalent number of gas channels/brick	12	
Number of brick/m^2	31.813	
Number of brick courses/stove	155	
Area share of the checkerwork in stove	75%	

The number of channels in the checkerwork was estimated by

$$N_{\mathrm{c,check}} = x_{\mathrm{check,stove}} \times A_{\mathrm{cross,stove}} \times \frac{N_{\mathrm{brick}}}{\mathrm{m}^2} \times N_{c,\mathrm{brick}} \tag{2}$$

where $N_{\mathrm{c,check}}$ is the number of channels in the checkerwork, $x_{\mathrm{check,stove}}$ is the area share of the checkerwork in the stove, $A_{\mathrm{cross,stove}}$ is the (radial) cross section area of the stove, N_{brick} is the number bricks required per unit area, and $N_{c,\mathrm{brick}}$ is the equivalent number of channels within a single brick.

3.2 Gas and Solid Temperature Model

The temperatures of the gas (blast or exhaust gas) and the brick are governed by the energy balance over a single tube. This can generally be modelled by a system of partial differential equations [8]:

Gas:
$$\rho_{\mathrm{g}} c_{\mathrm{p,g}} \left[\frac{\partial T_{\mathrm{g}}}{\partial t} + v_{\mathrm{g}} \frac{\partial T_{\mathrm{g}}}{\partial z}\right] + v_{\mathrm{g}} \frac{\partial P}{\partial z} = \frac{4h}{D_{\mathrm{h}}} (T_{\mathrm{w}} - T_{\mathrm{g}}) \tag{3}$$

Solid:
$$\rho_{\mathrm{s}} c_{\mathrm{p,s}} \frac{\partial T_{\mathrm{s}}}{\partial t} - \frac{1}{r}\frac{\partial}{\partial r}\left(r k_{\mathrm{s}} \frac{\partial T_{\mathrm{s}}}{\partial r}\right) - k_{\mathrm{s}} \frac{\partial^2 T_{\mathrm{s}}}{\partial z^2} = 0 \tag{4}$$

In the above equations, T_{g} and T_{s} are the gas and the solid temperature, v_{g} is the gas velocity, ρ_{g} and ρ_{s} are the gas and the solid density, $c_{\mathrm{p,g}}$ and $c_{\mathrm{p,s}}$ are the gas and the solid specific heat capacity, k_{s} is the thermal conductivity of the solid, P is the pressure, h is the gas-solid heat transfer coefficient, D_{h} is the hydraulic diameter of the gas channel, and T_{w} is the solid wall temperature. In Equation (3), the first and the second terms on the left-hand side represent the internal energy storing term and the rate of work done on the gas by pressure forces, while the term on the right-hand side refers to the energy flow by means of convective transport. In Equation (4), the terms on the left-hand side are the internal energy storing term, and heat flow by conductive transport in radial and axial direction respectively.

The boundary conditions for the gas and the solid in the above equations are

Gas:
$$\left.\frac{\mathrm{d}T_{\mathrm{g}}}{\mathrm{d}z}\right|_{z=z_{\mathrm{out}}} = 0 \tag{5a}$$

$$T_{\mathrm{g}}|_{z=z_{\mathrm{in}}} = T_{\mathrm{g,in}} \tag{5b}$$

Solid:

- Axial

$$\left.\frac{\mathrm{d}T_\mathrm{s}}{\mathrm{d}z}\right|_{z=0} = \left.\frac{\mathrm{d}T_\mathrm{s}}{\mathrm{d}z}\right|_{z=L} = 0 \tag{6a}$$

- Radial

$$\left.\frac{\mathrm{d}T_\mathrm{s}}{\mathrm{d}r}\right|_{r=r_\mathrm{i}} = \frac{2h}{k_\mathrm{s}(r_\mathrm{o}^2/r_\mathrm{i}^2 - 1)}(T_\mathrm{g} - T_\mathrm{s}|_{r=r_\mathrm{i}}) \tag{6b}$$

$$\left.\frac{\mathrm{d}T_\mathrm{s}}{\mathrm{d}r}\right|_{r=r_\mathrm{o}} = \frac{2h_\mathrm{loss}}{k_\mathrm{s}(1 - r_\mathrm{i}^2/r_\mathrm{o}^2)}(T_\mathrm{s}|_{r=r_\mathrm{o}} - T_\infty) \tag{6c}$$

In Equation (5), $z_\mathrm{in} = 0$ and $z_\mathrm{out} = L$ for the on-blast period, while $z_\mathrm{in} = L$ and $z_\mathrm{out} = 0$ for the on-gas period, and L is the total length of the channels, i.e., height of the checkerwork. The heat loss from the checkerwork was considered from each gas channel wall by Equation (6c), where the heat transfer coefficient h_loss was set to yield a reasonable over-all heat loss from the stove (cf. end of subsection 3.3).

This mathematical model is based on several assumptions:

1. The blast and the exhaust gas are treated as ideal gases.
2. Because of the low heat conductivity of the gas, the heat conduction of gas in axial direction is negligible and the gas-solid convection gives the dominant heat transfer in the system.
3. As the diameter of the gas channel is relatively very small compared to the height of the checkerwork, it is assumed that there is no gas temperature gradient in the radial direction.

To reduce the computation time, further simplifications are made to the model and are discussed in the following subsections. A brief derivation of the gas and solid temperature simplified model is provided in Appendix.

3.2.1 Simplification of the Gas Temperature Model

In this work, the effect of gas pressure gradient across the checkerwork length, $\frac{\partial P}{\partial z}$, to the energy balance was neglected. Therefore, the simplified gas temperature model is formulated as

$$\rho_\mathrm{g} c_\mathrm{p,g}\left[\frac{\partial T_\mathrm{g}}{\partial t} + v_\mathrm{g}\frac{\partial T_\mathrm{g}}{\partial z}\right] = \frac{4h}{D_\mathrm{h}}(T_\mathrm{w} - T_\mathrm{g}) \tag{7}$$

3.2.2 Simplification of the Solid Temperature Model

The radial temperature profile for the solid was briefly evaluated to examine its significance to the heat transfer in the system. By solving the simplified form of Equation (4) and Equation (7) over several cycles of alternating on-gas and on-blast phases, the radial temperature profile of the solid was obtained at quasi-stationary state. In this evaluation, the temperature of the incoming combustion gas temperature and the cold blast were arbitrarily fixed at 1300 °C and 150 °C respectively. In addition, the modelled thermal regenerator was assumed to be perfectly insulated at the outer radius, so the heat loss term was neglected. Figure 3.5 and Figure 3.6 show the radial temperature profile at the five uppermost and lowermost height segments after a typical on-gas and on-blast phase.

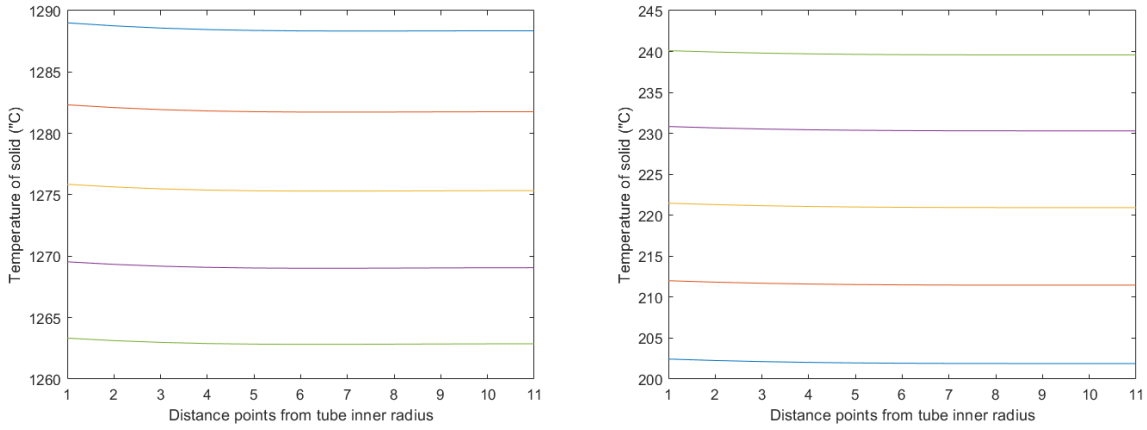

Figure 3.5 Solid temperature profile in radial direction of five uppermost segments (left) and five lowermost segments (right) of the modelled checkerwork after a typical on-gas phase

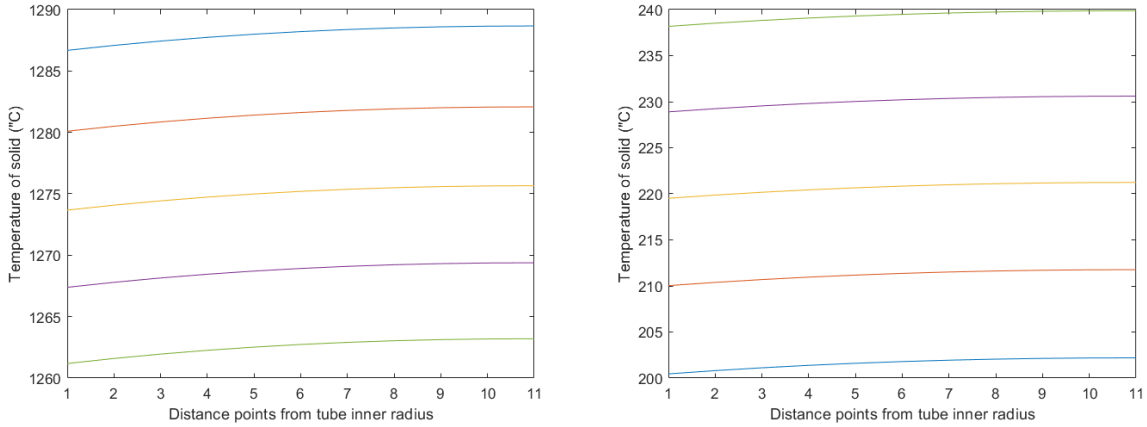

Figure 3.6 Solid temperature profile in radial direction of five uppermost segments (left) and five lowermost segments (right) of the modelled checkerwork after a typical on-blast phase

From the performed evaluation, it was found that the temperature variation of the solid in radial direction was below 1 °C and 3 °C at the end of the simulated on-gas phase and on-blast phase respectively. Even though the heat loss was not (yet) considered, it was estimated that it would not have considerable effect on the solid temperature profile in the radial direction. Therefore it was assumed that the checkers behave as a lumped parameter thermal system in the radial direction in the model, exactly as also done by Muske et al. [8] in their modeling work.

Based on the evaluation of heat transfer within the solid in the radial direction, the radial term in the energy balance partial differential equation for solid was neglected. Hence, the simplified temperature model for solid is described as

$$\rho_s c_{p,s} \frac{\partial T_s}{\partial t} - k_s \frac{\partial^2 T_s}{\partial z^2} = \frac{2h}{r_i(r_o^2/r_i^2 - 1)}(T_g - T_s) - \frac{2h_{loss}}{r_o(1 - r_i^2/r_o^2)} T_s \quad (8)$$

3.2.3 Final Simplified Model of Gas and Solid Temperature

To summarize, the final energy balance over the gas and the solid used in this work is presented below. The two partial differential equations are coupled in the gas-solid heat transfer term indicated with the presence of the heat transfer coefficient, h.

Gas:
$$\rho_{\mathrm{g}} c_{\mathrm{p,g}} \left[\frac{\partial T_{\mathrm{g}}}{\partial t} + v_{\mathrm{g}} \frac{\partial T_{\mathrm{g}}}{\partial z} \right] = \frac{4h}{D_{\mathrm{h}}} (T_{\mathrm{w}} - T_{\mathrm{g}}) \tag{9}$$

Solid:
$$\rho_{\mathrm{s}} c_{\mathrm{p,s}} \frac{\partial T_{\mathrm{s}}}{\partial t} - k_{\mathrm{s}} \frac{\partial^2 T_{\mathrm{s}}}{\partial z^2} = \frac{2h}{r_{\mathrm{i}}(r_{\mathrm{o}}^2/r_i^2 - 1)} (T_{\mathrm{g}} - T_{\mathrm{s}}) - \frac{2h_{\mathrm{loss}}}{r_{\mathrm{o}}(1 - r_{\mathrm{i}}^2/r_{\mathrm{o}}^2)} T_{\mathrm{s}} \tag{10}$$

The boundary conditions for the above equations are

Gas:
$$\left. \frac{\mathrm{d}T_{\mathrm{g}}}{\mathrm{d}z} \right|_{z=z_{\mathrm{out}}} = 0 \tag{11a}$$

$$T_{\mathrm{g}}\big|_{z=L} = T_{\mathrm{cg,in}} \quad \text{On-gas} \tag{11b}$$

$$T_{\mathrm{g}}\big|_{z=0} = T_{\mathrm{bl,in}} \quad \text{On-blast} \tag{11c}$$

$$T_{\mathrm{g}}\big|_{z=L} = T_{\mathrm{air,in}} \quad \text{Purging} \tag{11d}$$

Solid:
$$\left. \frac{\mathrm{d}T_{\mathrm{s}}}{\mathrm{d}z} \right|_{z=0} = \left. \frac{\mathrm{d}T_{\mathrm{s}}}{\mathrm{d}z} \right|_{z=L} = 0 \tag{12}$$

The initial condition for the solid is given by

$$T_{\mathrm{s}}(z, t=0) = f(z) \tag{13}$$

where the function $f(z)$ is arbitrary, but a previous solution of the solid temperatures can be used to speed up the convergence. According to [8], the effect of pressurization and blow-off on the checkerwork temperature during the switching/idle period before the on-blast and the on-gas cycle start, is small. Based on this, the gas-solid heat transfer during this period was neglected and that only heat loss is considered to affect the checkerwork temperature during this period.

3.3 Heat Transfer Parameters

3.3.1 Physical Properties of the Gas

The physical properties of the combustion gas and the blast at a certain time and position in the stove are determined based on the gas temperature, the gas composition, and temperature dependent physical properties of the gas components. The density of the gas is determined according to the ideal gas law

$$\rho_{\mathrm{m}} = \frac{P M_{\mathrm{m}}}{RT} \tag{14}$$

In this work, interpolating functions of physical properties for each component versus temperature from Zetterholm et.al. [1] were used to determine the specific heat capacity, thermal conductivity, and viscosity of the gas mixture. The physical properties data used in the interpolating functions referred to the available data by the National Institute of Standards and Technology (NIST) and Kjellström et.al. [14]. The specific heat capacity of the gas mixture is calculated based on component fraction in the gas mixture and individual component specific heat capacities according to

$$c_{\mathrm{p,m}} = \sum_{i=1}^{n} x_i c_{\mathrm{p},i} \tag{15}$$

where x_i is the mass fraction of component i and $c_{\mathrm{p},i}$ is the specific heat capacity of pure component i.

The viscosity of the gas mixture is estimated according to the method of Wilke, while the thermal conductivity of the gas mixture is determined using the method of Mason and Saxena [8]. The estimations of the viscosity and the thermal conductivity of the gas mixture are shown in Equations (17) and (18) respectively. Both calculations are based on the component fraction, the properties of individual components, and the interaction parameter between two species, $\phi_{i,j}$.

$$\phi_{i,j} = \frac{\left(1 + \left(\frac{\mu_i}{\mu_j}\right)^{\frac{1}{2}} \left(\frac{M_j}{M_i}\right)^{\frac{1}{4}}\right)^2}{\sqrt{8\left(1 + \frac{M_i}{M_j}\right)}} \tag{16}$$

$$\mu_{\mathrm{m}} = \sum_{i=1}^{n} \frac{y_i \mu_i}{\sum_{j=1}^{n} y_j \phi_{i,j}} \tag{17}$$

$$k_{\mathrm{m}} = \sum_{i=1}^{n} \frac{y_i k_i}{\sum_{j=1}^{n} 0.85 y_j \phi_{i,j}} \tag{18}$$

3.3.2 Gas Velocity and Mass Flowrate

The velocity of the gas passing through the channels is determined according to

$$v_{\mathrm{g}} = \frac{4\dot{m}_{\mathrm{g\,in}}}{\pi \rho_{\mathrm{g}} N_{\mathrm{c,check}} D_{\mathrm{h}}^2} \tag{19}$$

In the calculation for the hot-stove system without bypass, the mass flowrate of the gas during the on-gas phase and mass flowrate of the blast during the on-blast phase are constant. In this configuration, during the on-blast stage, the temperature of the hot blast at the outlet of the checkerwork naturally declines as time progresses due to the depletion of the thermal energy stored in the checkerwork.

As for the hot-stove system with bypass, during the on-blast phase, the mass flow rate of the blast fed into the stove is controlled such that the final hot blast temperature can be maintained at the desired temperature required by the blast furnace. This is done by diverting a share of the cold blast flow and

mixing the diverted flow of cold blast with the outcoming hot blast from the stove. Based on the energy balance of the flows mixing, the mass flowrate fed into the stove can be theoretically calculated using

$$\dot{m}_{\mathrm{bl,in}} = \frac{\int_{T_{\mathrm{bl,in}}}^{T_{\mathrm{bl,tr}}} c_{\mathrm{p,g}} dT}{\int_{T_{\mathrm{bl,in}}}^{T_{\mathrm{bl,out}}} c_{\mathrm{p,g}} dT} \dot{m}_{\mathrm{bl,tot}} \tag{20}$$

where, $\dot{m}_{\mathrm{bl,tot}}$ is the total mass flowrate of the blast in the hot-stove system, $T_{\mathrm{bl,in}}$ and $T_{\mathrm{bl,out}}$ are the blast temperature at the inlet and the outlet of the stove respectively, and $T_{\mathrm{bl,tr}}$ is the target temperature of the hot blast after mixing of hot blast from the stove and bypass air.

The share of the cold blast that shall flow into the stove at any given time can be estimated from an energy balance equation. Assuming that the gas specific heat capacity is approximately constant on average, we get

$$x_{\mathrm{bl,in}} = \frac{T_{\mathrm{bl,tr}} - T_{\mathrm{bl,in}}}{T_{\mathrm{bl,out}} - T_{\mathrm{bl,in}}} \tag{21}$$

3.3.3 Heat Transfer Coefficients

During the on-gas cycle, both convective and radiative heat transfer contribute to the overall heat transfer. This is due to the presence of a considerable fraction of carbon dioxide and water vapor in the combustion gas. During the on-blast cycle, radiative heat transfer might also take place beside the convective heat transfer. However, since the content of carbon dioxide and water vapor in the cold blast is relatively small, only convective heat transfer is considered during the on-blast cycle. The total heat transfer coefficients for the on-gas and the on-blast cycle are described as

$$h_{\mathrm{heat}} = h_{\mathrm{conv}} + h_{\mathrm{rad}}$$
$$h_{\mathrm{blast}} = h_{\mathrm{conv}}$$

The coefficient of the convective heat transfer, h_{conv}, during on-gas cycle and on-blast cycle is estimated from the Nusselt number. In this work, the correlation used to determine the Nusselt number for flow inside long circular tubes is [4]

$$Nu = 0.023\, Re^{0.8} Pr^{\frac{1}{3}} \tag{22}$$

$$Re = \frac{\rho_{\mathrm{g}} v_{\mathrm{g}} D_{\mathrm{h}}}{\mu_{\mathrm{g}}} \tag{23}$$

$$Pr = \frac{\mu_{\mathrm{g}} c_{\mathrm{p,g}}}{k_{\mathrm{g}}} \tag{24}$$

The correlation in Equation (22) is valid for $Re > 10^4$ and $0.7 < Pr < 120$. Even though the Reynolds number for the gas and blast flow in the studied hot-stove system is smaller than 10^4, this correlation was nevertheless used for approximate estimation.

Based on the above relationships, the convective heat transfer coefficient is

$$h_{\mathrm{conv}} = \frac{Nu\, k_{\mathrm{g}}}{D_{\mathrm{h}}} \tag{25}$$

Beside the range of operating temperature, the radiative heat transfer from a gas to a surface is mostly determined by the content of the radiating species in the gas, which are CO_2 and H_2O. The radiation from the CO_2 and H_2O in the hot combustion gas to the checker channel surface can contribute by up to 20% of the total heat transferred during the on-gas cycle [8]. In this case, the checker channel surface is treated as a grey, opaque, diffuse surface. The heat radiation from combustion gas to the surface of the checker channels can, therefore, be described by Equation (26) [1], which assumes symmetrical gas geometry in an infinite long cylinder.

$$\dot{Q}_{\mathrm{rad}} = \frac{\epsilon_{\mathrm{s}}\sigma(\epsilon_{\mathrm{g}}T_{\mathrm{g}}^4 - \alpha_{\mathrm{g}}T_{\mathrm{s}}^4)}{1-(1-\alpha_{\mathrm{g}})(1-\epsilon_{\mathrm{s}})} \tag{26}$$

The emissivity of the checker channel surface was estimated to be $\epsilon_{\mathrm{s}} = 0.8$ [8] while the total emissivity and absorptivity of the gas, ϵ_{g} and α_{g}, were estimated by using the method of Hottel. The method of Hottel uses the correlation between the gas temperature, the gas total pressure, the partial pressure of the radiating species, and the beam length of the gas geometry. Since the ratio between the channel diameter to the checkerwork length is very small, it is assumed that the prevailing heat radiation is towards the curved surface of the gas channel. Therefore, the characteristic length for the heat radiation is defined as the diameter of the channel, D_h, and the mean beam length is set as 0.95 D_{h} [15].

Based on the above considerations, the radiative heat transfer coefficient is approximated as

$$h_{\mathrm{rad}} = \frac{\epsilon_{\mathrm{s}}\sigma(\epsilon_{\mathrm{g}}T_{\mathrm{g}}^4 - \alpha_{\mathrm{g}}T_{\mathrm{s}}^4)}{1-(1-\alpha_{\mathrm{g}})(1-\epsilon_{\mathrm{s}})}\frac{1}{T_{\mathrm{g}}-T_{\mathrm{s}}} \tag{27}$$

According to the stove heat loss evaluation performed by Nyman [4] in 2014 at SSAB Raahe, the average heat loss rate from stove #3 for BF2 to the surrounding , was found to be $\bar{Q}_{\mathrm{loss}} \approx 600$ kW. This value was obtained based on the measurement of surface temperature of the stove. By assuming that the average heat loss rate stays at this level, and that all of the heat loss comes from the checkerwork, the coefficient of heat loss to the surrounding for one checker channel was approximated as

$$h_{\mathrm{loss}} = \frac{\bar{Q}_{\mathrm{loss}}}{N_{\mathrm{c,check}}\, A_{\mathrm{c,outer}}\, \overline{T_{\mathrm{s}}}} \tag{28}$$

3.4 Model Solution Technique

The simplified model of the gas and solid energy balances was solved numerically using the pdepe solver in MATLAB. This solver implements the method of lines together with a finite element discretization in space, i.e., the spatial derivatives are discretized while the time derivatives are held continuous [16]. Therefore, the internal time step is variable and progresses according to the fixed tolerance level, but results can be required at suitable time moments (e.g., at given steps in time).

3.5 Simulation of Hot-Stove System

3.5.1 Combustion Calculation

Before starting the main simulation of the hot stoves, the calculation of fuel combustion is done to determine the state of combustion gas entering the checkerwork during the on-gas cycle. The following assumptions are made to simplify the calculation.

1. The composition of the supplied fuel gas, i.e., blast furnace top gas with or without addition of external fuel, is constant.
2. Fuel and air are perfectly mixed in all local regions inside the combustion chamber, resulting in complete combustion.
3. The combustion air is assumed to be dry, with the composition of 79% N_2 and 21% O_2. The flowrate of the combustion air is estimated from the air excess factor, which is approximated from the target O_2 content in the exhaust gas.
4. The combustion takes place under adiabatic conditions
5. The combustion is assumed to be complete and any C and H in the fuel is converted into CO_2 and H_2O.

The air excess factor, λ, can be briefly estimated using target value of the O_2 concentration in dry combustion gas [14]

$$\lambda = \frac{y_{\mathrm{O_2,d}}}{0.21 - y_{\mathrm{O_2,d}}} \frac{\dot{n}_{\mathrm{cg,stoic}}}{\dot{n}_{\mathrm{ca,stoic}}} \tag{29}$$

The temperature of the combustion gas is predicted by solving the general energy balance for combustion as described by

$$\begin{gathered} \dot{m}_{\mathrm{cg}} h_{\mathrm{cg}} = \dot{m}_{\mathrm{ca}} h_{\mathrm{ca}} + \dot{m}_{\mathrm{fuel}} (H_{\mathrm{fuel}} + h_{\mathrm{fuel}}) \\ h_{\mathrm{cg}} = f(T_{\mathrm{cg}}) \end{gathered} \tag{30}$$

3.5.2 Hot-stove Main Simulation

In this work, the hot-stove system was simulated based on the formulated heat transfer models. The calculation is performed for every hot stove in the system and through a sequence according to the operation of the hot stoves as described in Chapter 2.

To enable a continuous flow of hot blast to the blast furnace, the total cycle length is the sum of the durations of on-blast times of the n hot stoves in the system. Provided that the time required to complete the purging and switching stages are identical for each stove in the system, the length of the on-gas period for each stove can be determined according to

$$t_{\mathrm{heat},i} = \sum_{i=1}^{n} t_{\mathrm{blast},i} - t_{\mathrm{switch\ tot},i} - t_{\mathrm{purge},i} \tag{31}$$

The simulation of the stove system was done according to the desired number of steps or until a convergence criterion was satisfied, expressing that the system has stabilized to reach a quasi-stationary state. In this work, some assumptions that were made when performing the simulation are listed below:

1. The incoming flows of combustion gas and blast were assumed to have constant temperature at the boundary, constant composition, and constant mass flowrate over the simulated period.
2. The length of purging and switching periods was kept constant for each stove regardless of different on-gas and on-blast cycle periods.

Based on the simulation procedure described above, the temperature profiles of gas and solid over the simulated period and along the checkerwork height are solved.

The input data required to run the main simulation are listed in Table 3.2 and Table 3.3.

Table 3.2 Required process flow data

Process flow	Parameter
Cold blast	$\dot{V}$, T, p, composition
Blast furnace top gas	$\dot{V}$, T, p, composition
COG/external fuel	Composition
Exhaust gas	O_2 content

Table 3.3 Required operation parameter data

Operation parameter
$t_{\mathrm{blast},i}$
t_{switch}
t_{purge}
$T_{\mathrm{bl,tr}}$

In this work, the initial temperatures of the checkerwork matrix assigned in the beginning of the simulations are given by a linear function

$$T_{\mathrm{s}}(z, t=0) = \left[1100 - \frac{z}{N_{\mathrm{step,z}}} \times 900\right] ℃ \tag{32}$$

where, z is the spatial interval where the temperature is being assigned and $N_{\mathrm{step,z}}$ is the number of spatial steps across the discretized checkerwork height. While the checkerwork initial temperature could possibly affect the number of cycles required before quasi-steady state is reached, any starting point can be used, nevertheless.

3.6 Optimization of the Hot-stove System

Using the simulation procedure, the possibility to optimize the hot-stove system performance was investigated. The objective is to identify the operation conditions that enable as high final blast temperature as possible and/or minimize the consumption of fuel. The optimization problem for maximizing the blast temperature can be written as

$$\min_{\boldsymbol{x}} \{F = -T_{\mathrm{bl,end}}\} \tag{33}$$

subject to

$$T_{\mathrm{s},i}(t, N) \leq T_{\mathrm{h,max}} \; ; \quad \forall i \, , t \in \mathcal{K}_{\mathrm{qss}} \tag{34a}$$

$$T_{\mathrm{s},i}(t, 1) \leq T_{\mathrm{c,max}} \; ; \quad \forall i \, , t \in \mathcal{K}_{\mathrm{qss}} \tag{34b}$$

In Equation (33), $\boldsymbol{x}$ refers to a vector of manipulated variables, which in this work includes the duration of the on-blast cycle of each stove, final hot blast temperature set point, and the share of external fuel. In Equation (34), indices 1 and N refer to the first and the last segment of the discretized checkerwork

length, i refers to the stove number, and $\mathcal{K}_{\mathrm{qss}}$ is the set of time steps in a hot stove cycle at quasi-stationary state operation. The constraints in Equation (34a) and (34b) express some temperature limits for the checkerwork operating at quasi-stationary state. The temperature of the dome after the combustion chamber should not exceed a maximum allowable value ($T_{\mathrm{h,max}}$) to prevent brickwork damage. In addition, an upper limit for the temperature at the cold end of the stoves ($T_{\mathrm{c,max}}$) is usually imposed to avoid damage to the support structures of the checkerworks [12]. Note that the constraints here are set arbitrarily and do not necessarily correspond to those applied in the industry.

The pressure loss over the hot stove, which is dictated by the gas pipeline and gas holder pressure, could also be included as one of the constraints limiting the feasible solution. However, it is not considered here since pressure loss was not modelled in this work.

4 Results and Discussion

This chapter presents some results of combustion calculation and simulation of the hot stove system. Simulations of different cases of hot-stove systems with and without bypass were done with the focus to evaluate the typical thermal behavior of system at various operating conditions, to investigate the extent of the effects given by the contributing variables in the operation, as well as to search for possibilities to optimize the system.

4.1 Combustion of Fuel Gas

Before the hot stove simulations were performed, the combustion of the fuel gas was evaluated to determine the state of the gas that is fed into the hot stoves and that heats up the checkerwork during the on-gas stage. Table 4.1 shows the default input data used in the combustion calculations in this work.

Table 4.1 General input data used in the combustion calculation

Parameter	Value	Unit	Note
$\bar{V}_{\mathrm{TG},i}$	41.3	kNm^3/h	Average top gas rate per stove
$y_{\mathrm{CO,TG}}$	21.6	%	
$y_{\mathrm{CO_2,TG}}$	24	%	
$y_{\mathrm{H_2,TG}}$	2.8	%	
$y_{\mathrm{N_2},TG}$	49.6	%	
$y_{\mathrm{H_2O\_v,TG}}$	2	%	
$y_{\mathrm{H_2O\_l,TG}}$	3	g/m^3	Top gas after gas cleaning
T_{fuel}	35	°C	Combustion fuel mixture
T_{ca}	10	°C	
$y_{\mathrm{O_2,ca}}$	2	%	

For the given top gas composition, the heating value of the top gas is approximately 3 MJ/m^{3}n. Based on the calculation performed using the input data in Table 4.1, it was estimated that the combustion air excess factor, λ, of the studied hot-stove system is around 0.26 and the temperature of the combustion gas is about 1160 °C. Apparently, the estimated λ is quite high as the typical air factor, (1+ λ), for gas burner is within the range of 1.05 to 1.1 [14]. However, the estimated λ in this study could be overestimated, since a theoretical approach was taken in the calculation. To illustrate the discrepancies that potentially arise due to this approach, the typical relationship between the component fractions in the combustion gas versus the air factor in both theoretical and real combustion is depicted in Figure 4.1.

According to Figure 4.1, theoretically, stoichiometric combustion ($\lambda = 0$) yields no O_2 in the combustion gas. However, in reality, there is some O_2 present in the gas product of the combustion, because it is almost impossible to have perfect fuel-air mixing in all local regions in the combustion chamber. In this work, λ was calculated based on the measured O_2 content in the combustion gas, while it was assumed that the combustion occurs ideally. Because of this, the estimated λ might be too high and, therefore, the predicted temperature of the combustion gas could possibly be lower than it is in reality.

To approach better accuracy in determining the temperature of the combustion gas entering the checkerwork, temperature measurements of the gas, e.g. at the stove dome, can be helpful. In addition, measurement data of combustion air flowrate and analysis of CO_2 and CO content in the combustion gas, if available, can also be beneficial to verify the accuracy of the combustion model.

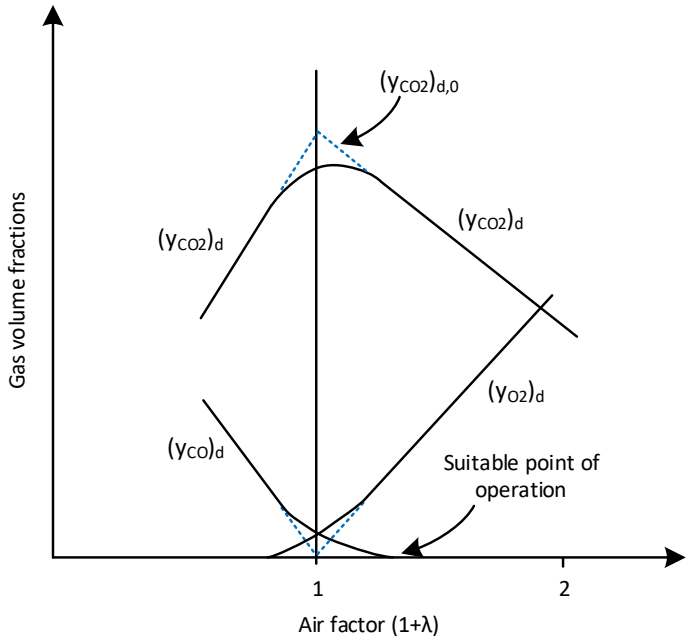

Figure 4.1 Illustrative schematic of relationship between CO_2, CO, and O_2 contents and air factor in theoretical (dashed lines) and real (solid lines) combustion [14]

4.2 Simulation of Hot-stove System

In this work, the system simulated consists of three hot stoves ($n = 3$). A spatial step of about 0.4 m was used in the checkerworks and the solution was taken out for every 10 seconds. For each case, the simulation was done for 30 full stove cycles, as it adequately satisfies the fixed convergence criterion of quasi-stationary state for all cases. In this study, the systems are assumed to have reached the quasi-stationary state when the difference of the hot blast temperatures between two consecutive cycles is below 1 °C.

A brief energy balance evaluation over the solid and gas in the modelled checkerwork was first performed for a system with identical hot stoves and without bypass, with the purpose of verifying the model's reliability. Only for this energy balance check, the heat loss is not considered. The energy balance was evaluated at the end of an on-gas and an on-blast phase at quasi-stationary state, and was calculated as [8]

$$E_\mathrm{s} = \int_0^L N_\mathrm{c,check}\,\pi\left(r_\mathrm{o}^2 - r_\mathrm{i}^2\right)\rho_\mathrm{s}\left(\int_{T_\mathrm{s,init}}^{T_\mathrm{s,end}} c_\mathrm{p,s}\,\mathrm{d}T\right)\mathrm{d}z \tag{35}$$

$$E_\mathrm{g} = \int_0^{t_\mathrm{phase}} \dot{m}_g\left(\int_{T_\mathrm{g,in}}^{T_\mathrm{g,out}} c_\mathrm{p,g}\,\mathrm{d}T\right)\mathrm{d}t \tag{36}$$

$$E_\mathrm{error} = \frac{E_\mathrm{s} + E_\mathrm{g}}{|E_\mathrm{s}|} \times 100\% \tag{37}$$

where E_s and E_g are the energy gained/discharged by the solid and the gas, $T_\mathrm{s,init}$ and $T_\mathrm{s,end}$ are the checkerwork temperature at the beginning and at the end of the on-gas/on-blast stage and E_error is the

relative percentage of error in the energy balance. Based on the evaluation, for the spatial step size used in the simulation, $E_{\text{error}} \approx 0.9\%$ for the on-gas and $E_{\text{error}} \approx 0.7\%$ for the on-blast stage, respectively. Thus, the model must be deemed fairly accurate. Spatial discretization using finer increment and setting smaller time step size can reduce the errors, but this will also require longer computation time.

The general parameters used in the simulation are listed in Table 4.2. In addition, the simulation in this work assumes a period of blast flow transition during the first two minutes and the last two minutes of each on-blast period. As for the parameters related with combustion calculation, the data from Table 4.1 is used unless otherwise specified.

Table 4.2 General parameters for the hot-stove system simulation

Parameter	Value	Unit	Note
$\dot{V}_{\text{bl}}$	140	kNm^3/h	
p_{bl}	3.5	bar	Blast pressure after compressor
$T_{\text{bl,in}}$	150	°C	Blast temperature after compressor
$t_{\text{switch}-\text{bh}}$	3	min	Blast to heat switching time
$t_{\text{switch}-\text{hb}}$	6	min	Heat to blast switching time
t_{purge}	1	min	

The results of the simulation are the estimated temperatures of the gas (the combustion gas and the hot blast) and the solid (the checkerwork bricks) within the defined range of position and time. Among the variables of interest to be evaluated from the simulation results are the hot blast temperature at the stove outlet ($T_{\text{bl,out}}$), and the final hot blast temperature ($T_{\text{bl,end}}$) which is the temperature of the combustion air in the blast furnace. It is desirable that the hot-stove system is capable to deliver hot blast with a stable and as high temperature as possible within the range of 1000-1250 °C. In addition, it is important that the solid temperatures, T_{s}, at both the hot end ($T_{\text{s,N}}$) and the cold end of the checkerwork ($T_{\text{s},1}$) are maintained below the maximum allowable temperatures, which in this work are limited to 1300 °C at the hot end and 350 °C at the cold end.

In general, it can be expected that the variables affecting $T_{\text{bl,end}}$ and T_{s} include: (1) the duration of full cycles of the stoves (t_{cyc}), which is determined by the length of on-blast period of each stove in the system, (2) the combustion fuel level, and (3) the combustion fuel heating value, which depends on the composition of the top gas and the addition of external fuel. There are many possible scenarios with different operating conditions of the hot-stove system. In this work, several cases were studied and will be discussed in the next sections. These case studies are chosen to reflect how the hot stoves characteristics, the bypass configuration, and the system operation variables influence the performance of the entire hot-stove system.

4.2.1 System of Identical Hot Stoves without Bypass

Case 1 – System of Hot Stoves of Identical Characteristics and Equal On-blast Periods

In this section, hot stoves of identical characteristics and equal on-blast periods in a system without bypass is studied. The parameters used are listed in Table 4.3. Here, the parameters related to fuel were set to default, with maximum fuel rate ($f_{\text{fuel}} = 1$) and no addition of external fuel ($x_{\text{ext fuel}} = 0$). Figure 4.2 shows the hot blast temperature evolution during the first 20 cycles (transient state) while the results of the thermal behavior of the system at quasi-steady state are shown in Figure 4.3 to Figure 4.6.

Table 4.3 Simulation parameters for Case 1

Parameter	Unit	Case 1
$\eta_1 = \eta_2 = \eta_3$	-	1
$t_{\text{blast},1} = t_{\text{blast},2} = t_{\text{blast},3}$	min	60
t_{cyc}	min	180
f_{fuel}	-	1
$x_{\text{ext fuel}}$	-	0

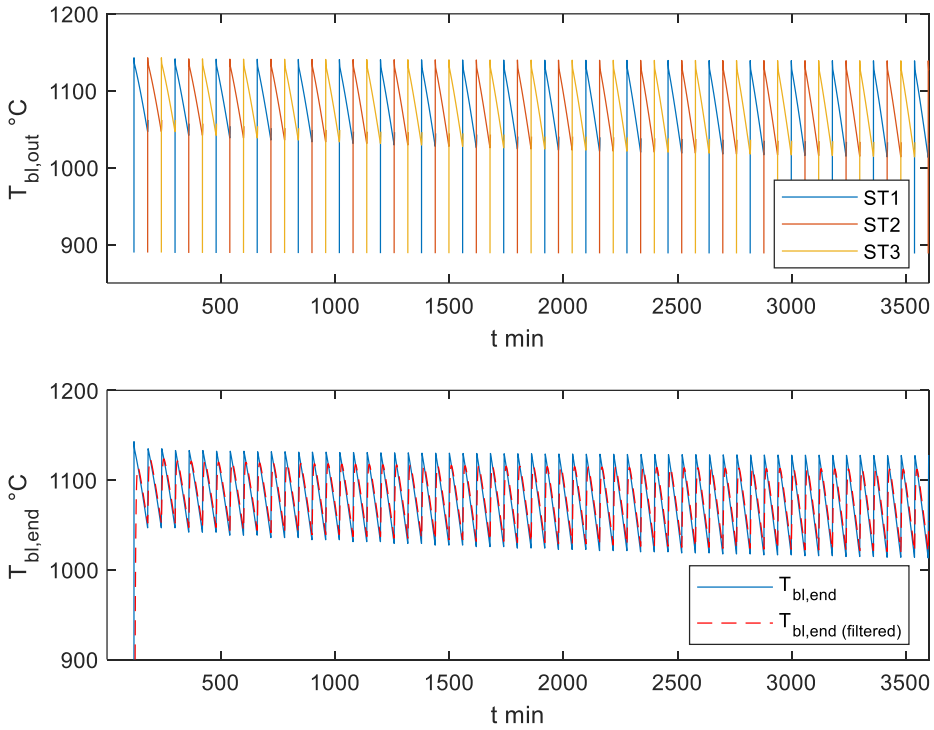

Figure 4.2 Evolution of blast temperature during the first 20 cycles for Case 1

The upper panel of Figure 4.3 shows the temperature of the hot blast flowing out of each individual stove ($T_{\text{bl,out}}$) in the system throughout the operation at quasi-stationary state. Note that the mass flow rate of the hot blast right after the stove is not constant as there are flow ramps-up and -down during the blast transition phase, i.e., the first two minutes and the last two minutes of the on-blast stages. It can be observed that $T_{\text{bl,out}}$ starts from a quite low temperature during the transition when the on-blast phase commences. This is likely due to the low heat transfer coefficient during the pre-blast transition phase (the first two minutes of the on-blast stage), as depicted in Figure 4.4. The convective heat transfer coefficient is dictated by the velocity of the gas, which is dependent on the mass flowrate. On the other hand, mass flowrate of the blast also determines the energy balance during the gas-solid heat exchange. As the blast flow ramps down during the post-blast transition phase, there is less blast available to carry the enthalpy, which results in a slight rise in $T_{\text{bl,out}}$.

The bottom panel of Figure 4.3 presents the final temperature profile of the total hot blast after mixing of the flows from the stoves ($T_{\text{bl,end}}$). The simulation result predicted that $T_{\text{bl,end}}$ from the system decreases from 1125 °C to 1008 °C throughout the 60 minutes of the on-blast period. This reflects the depletion of the thermal energy stored in the checkerwork as it keeps giving off heat to the cold blast during the on-blast phase. $T_{\text{bl,end}}$ read by a slow thermocouple (behaving as a first order system) may show somewhat narrower temperature range than the real temperature range, as illustrated by the red dashed line.

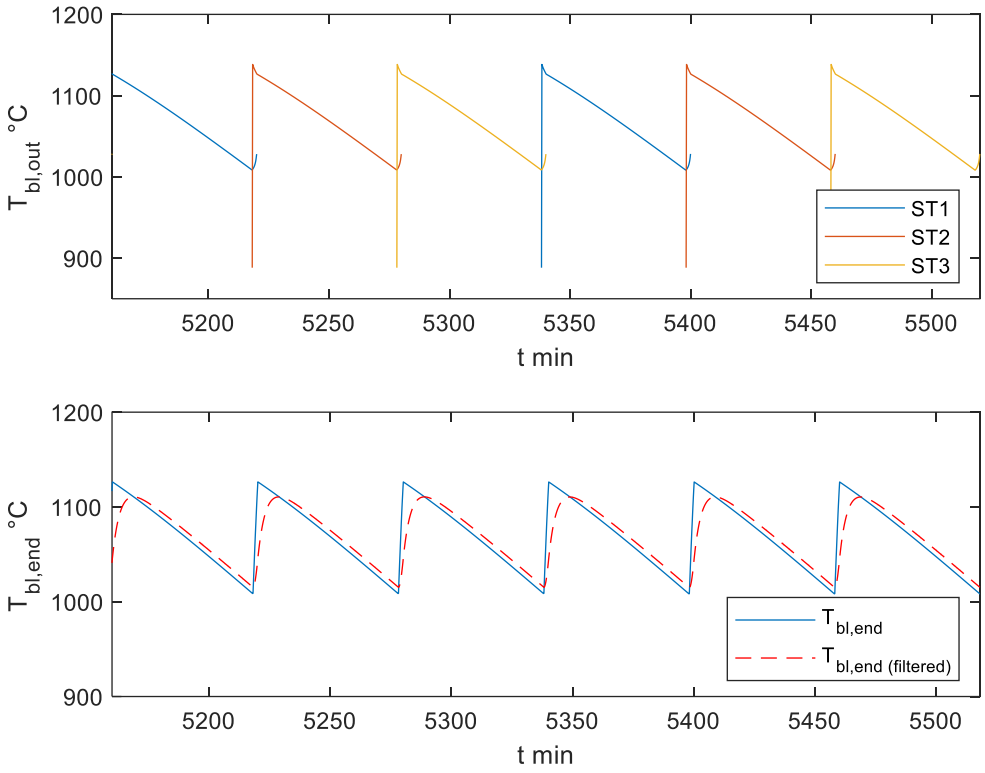

Figure 4.3 Predicted temperature of the hot blast after the stoves (top) and predicted temperature of final blast after flows mixing (bottom) at quasi-steady state for Case 1

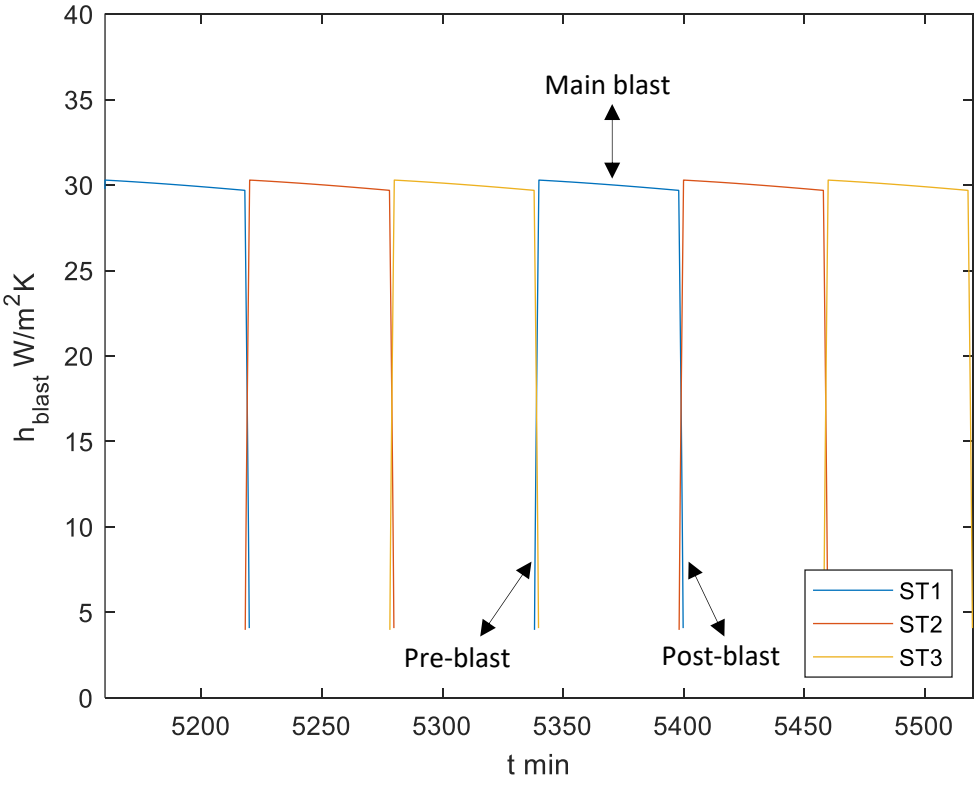

Figure 4.4 Predicted gas-solid heat transfer coefficient during on-blast stage at quasi-steady state for Case 1

Figure 4.5 depicts how the temperature of the checkerwork hot end and cold end evolve throughout the cycles at quasi-stationary state operation. Considerable changes can be observed especially in the checkerwork temperature at the hot end, or the uppermost segment of the checkerwork ($T_{s,N}$). From the top panel of Figure 4.5, it can be seen that during the stove heating phase (A), $T_{s,N}$ rises to a high temperature close to combustion gas temperature. The temperature then slightly decreases during the short period of purging (B) where the remaining combustion gas inside the stove is flushed out by an air flow. When the stove is switched (C) to prepare for the on-blast stage, $T_{s,N}$ stays relatively constant. $T_{s,N}$ then decreases throughout the on-blast period (D), and when the stove has finished the on-blast stage, it is switched (E) to heating stage and starts over the cycle.

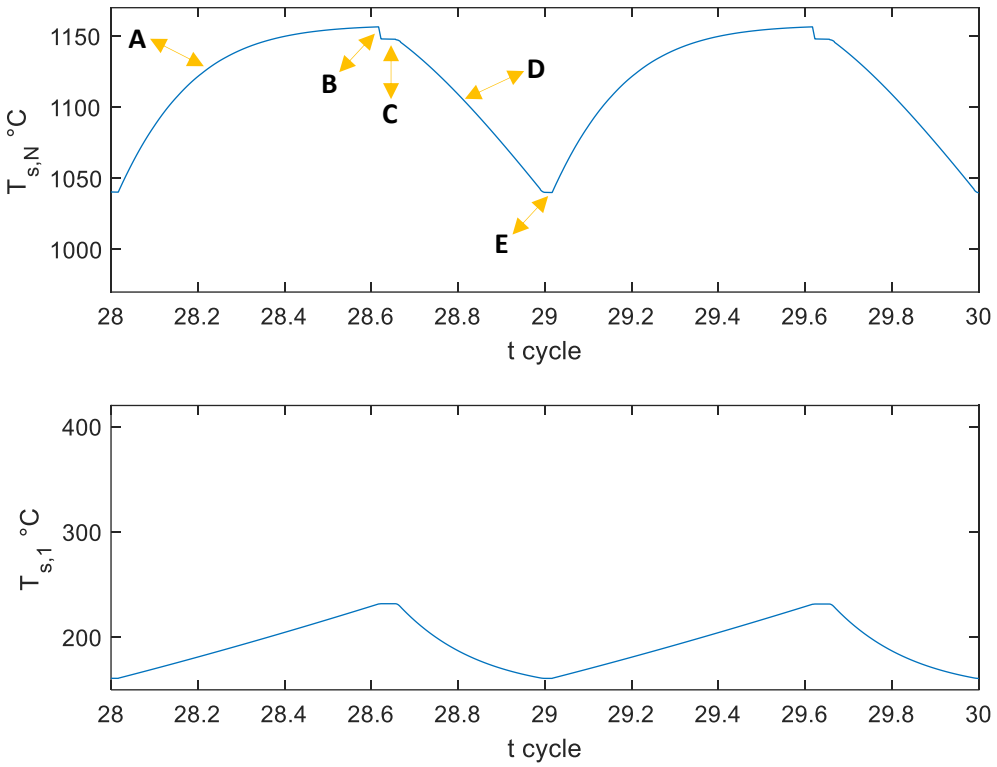

Figure 4.5 Predicted temperature of solid at the hot end (top) and the cold end (bottom) of the checkerwork at quasi-steady state for Case 1

Over one full cycle (180 minutes), the simulation predicted that T_s at the hot end and the cold end of the checkerwork vary from 1156 °C to 1040 °C and from 231 °C to 161 °C respectively. As depicted in Figure 4.6, the temperature of the checkerwork at the inlet boundary became reasonably close to the temperature of the gas and the blast flowing into the stove at the end of the on-gas and the on-blast phase respectively.

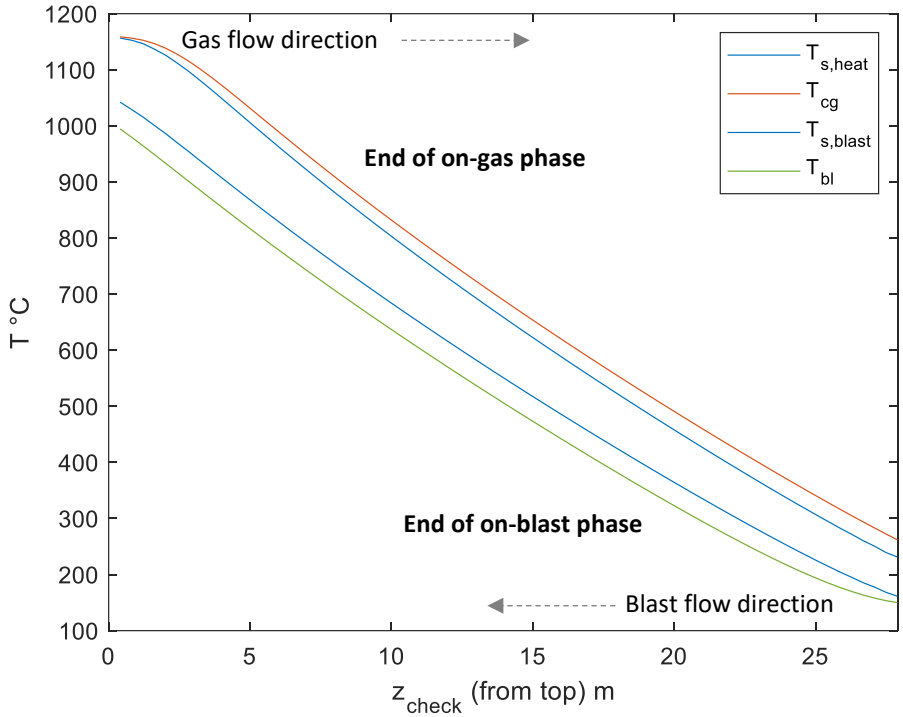

Figure 4.6 Typical vertical temperature profile in the checkerwork at the end of on-gas cycle (two lines at top) and on-blast cycle (two lines at bottom)

Effect of the Duration of Full Cycle on the Final Blast Temperature

The duration of one full cycle (t_{cyc}) of the hot-stove system governs the on-blast phase period (t_{blast}) and the on-gas phase period (t_{heat}) for each stove, which in turn rules $T_{\mathrm{bl,end}}$. At a longer full cycle time, t_{heat} also becomes longer, leading to more thermal energy stored in the checkerwork. On the other hand, this effect might be inherently counterbalanced since also t_{blast} becomes extended at a prolonged full cycle time, which may result in larger temperature decrease during the on-blast cycle and thus lowering $T_{\mathrm{bl,end}}$ at the end of the on-blast cycle.

For systems of hot stoves with equally long on-blast period for each stove, the predicted effect of the on-blast period of 30-90 minutes, i.e., full cycle length of 90-270 minutes, on the lowest final blast temperature at the end of the on-blast period ($T_{\mathrm{bl,end}}^{\mathrm{min}}$) is captured in Figure 4.7.

The highest $T_{\mathrm{bl,end}}^{\mathrm{min}} \approx 1011℃$ is achieved at $t_{\mathrm{blast}} \approx 80$ min, i.e., $t_{\mathrm{cyc}} \approx 240$ min and $t_{\mathrm{heat}} \approx 160$ min. For $t_{\mathrm{blast}} > 80$ min, the lowest final blast temperature is estimated to start declining. This could be due to the fact that the checkerwork has a limited heat storing capacity, so it starts to get thermally saturated during the on-gas phase when it is heated for a period longer than 160 minutes and with the temperature of the combustion gas predicted in Case 1 (cf. two upper curves in Figure 4.6). The upper part of the checkerwork reaches a temperature close to the temperature of the combustion gas, hence lowering the heat transfer rate. Furthermore, assuming that the checkerwork cooling rate during the on-blast cycle is somewhat constant due to the constant cold blast flow rate through the checkerwork, more thermal energy is discharged from the checkerwork at an extended t_{blast} whereas the available thermal energy at the beginning of the on-blast period is approximately at the same level.

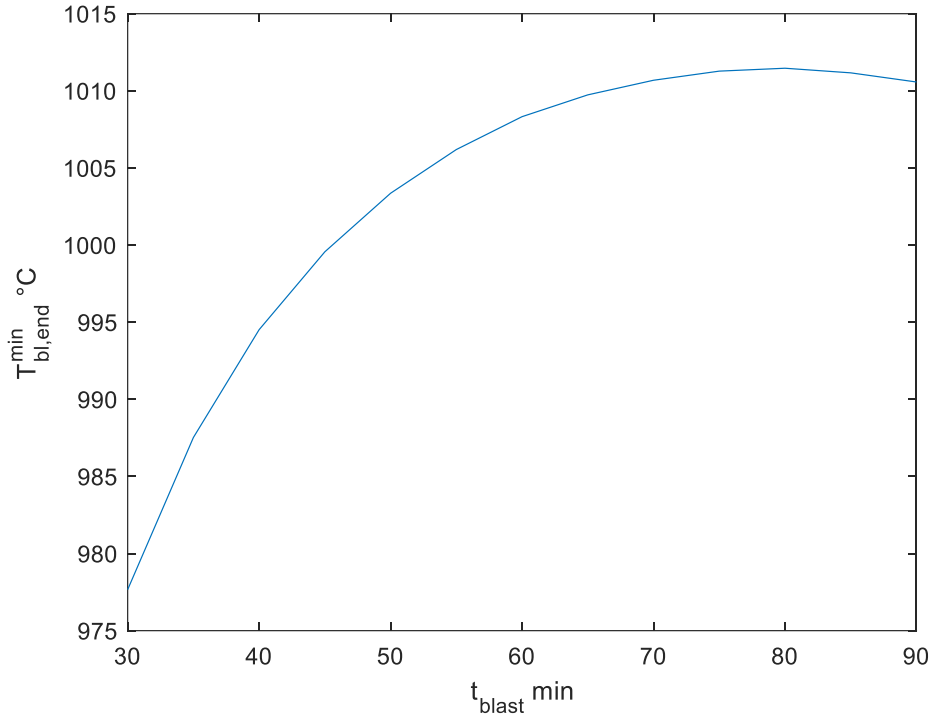

Figure 4.7 Predicted final lowest blast temperature as function of full cycle lengths for systems with hot stoves of equally long on-blast periods

Figure 4.8 illustrates the estimated maximum temperature reached at the checkerwork cold end ($T_{s,1}^{max}$) of a hot-stove system with identical on-blast periods at various full cycle durations. With the parameters applied in this case, $T_{s,1}^{max}$ varies practically linearly with t_{cyc}.

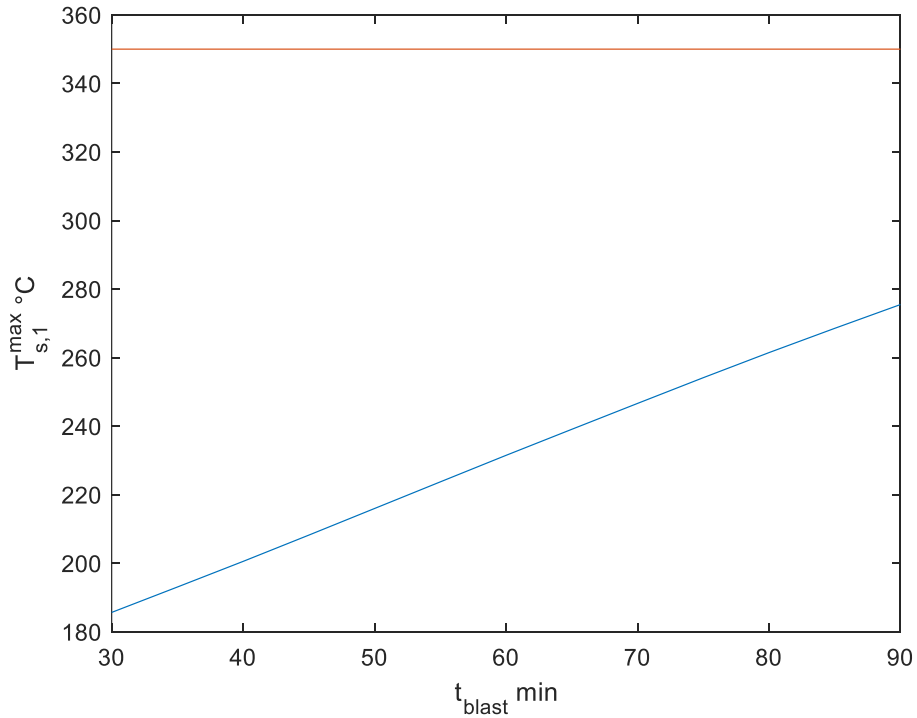

Figure 4.8 Predicted maximum temperature of solid at the cold end of the checkerwork as function of full cycle lengths for systems with hot stoves of equally long on-blast periods

4.2.2 System of Hot Stoves of Different Characteristics without Bypass

In reality, each stove has different characteristics due to many factors including different ages (except for greenfield plants) due to different revamping history of the stoves. Furthermore, the stoves may have different checkerwork materials or different control system responsiveness. The first alternative is still the most common reason for the differences: channels may be partially or fully clogged because of soot or particulate deposition, which decreases the available heat transfer surfaces in the checkerworks, or even melting due to occasional operation under too high temperatures (e.g., caused by excessive flame lengths). These factors can lower the efficiency of an individual stove and thus the overall performance of the hot-stove system.

In this section several cases of hot stoves of different characteristics in a system without bypass are evaluated. The parameters used in the simulation of those cases are listed in Table 4.4. A multiplying factor η, with value ranging from 0 to 1, was used to represent the different characteristics/efficiency of each stove and corresponds to the equivalent share of the checkerwork channels available for heat exchange. Therefore, a value of $\eta = 0.8$ is interpreted as a stove where only 80% of the channels are operating; thus, both the heat transfer surface and the available solid mass are decreased by 20% from the nominal values. It should also be stressed that the gas velocity in the channels increase correspondingly (cf. Equation (19)). In both Case 2A and 2B, the values of η were set as 1, 0.8, and 0.6 for Stove 1, 2, and 3 respectively. Whereas the on-blast periods were set to be identical for the stoves in Case 2A, the on-blast periods were varied in accordance with the characteristics of the stoves in Case 2B.

Table 4.4 Simulation parameters for Case 2

Parameter	Unit	Case 2A	Case 2B
η_1	-	1	1
η_2	-	0.8	0.8
η_3	-	0.6	0.6
$t_{\mathrm{blast},1}$	min	60	62
$t_{\mathrm{blast},2}$	min	60	60
$t_{\mathrm{blast},3}$	min	60	58
t_{cyc}	min	180	180
f_{fuel}	-	1	1
$x_{\mathrm{ext\ fuel}}$	-	0	0

Case 2A – System of Hot Stoves of Different Characteristics and Equal On-blast Periods

Figure 4.9 illustrates the approach to quasi-stationary state of a stove set with the characteristics of Case 2A. Further scrutiny of the results reveals that the difference in stoves characteristics can be noticed in the blast temperature particularly at the end of the on-blast period, as $t_{\mathrm{blast},i}$ for each stove is equal. According to Figure 4.10 and Figure 4.11, the temperature of the hot blast from the most deteriorated stove is dragged down to 941 °C at the end of its on-blast period, while the last temperature of the hot blast from the other two stoves are still around 1009 °C and 983 °C at the end of their on-blast stages. It can also be observed from Figure 4.10 (upper panel) that the different physical characteristics of the stoves also have some influence on the predicted initial T_{blast} at the beginning of the on-blast phase.

According to simulated temperature profile of the checkerworks depicted in Figure 4.11, it can be observed that when a hot stove's performance is deteriorated, it becomes undersized for its designed

operating condition. This is shown by T_s at both the hot end and the cold end of the checkerwork. As the checkerwork is heated more rapidly during the on-gas period, it is also cooled down faster during the on-blast phase in comparison with the other stoves with better characteristics. Because of this, some local hot spots at the bottom part of the checkerwork may appear in the case where the stove's channels are clogged.

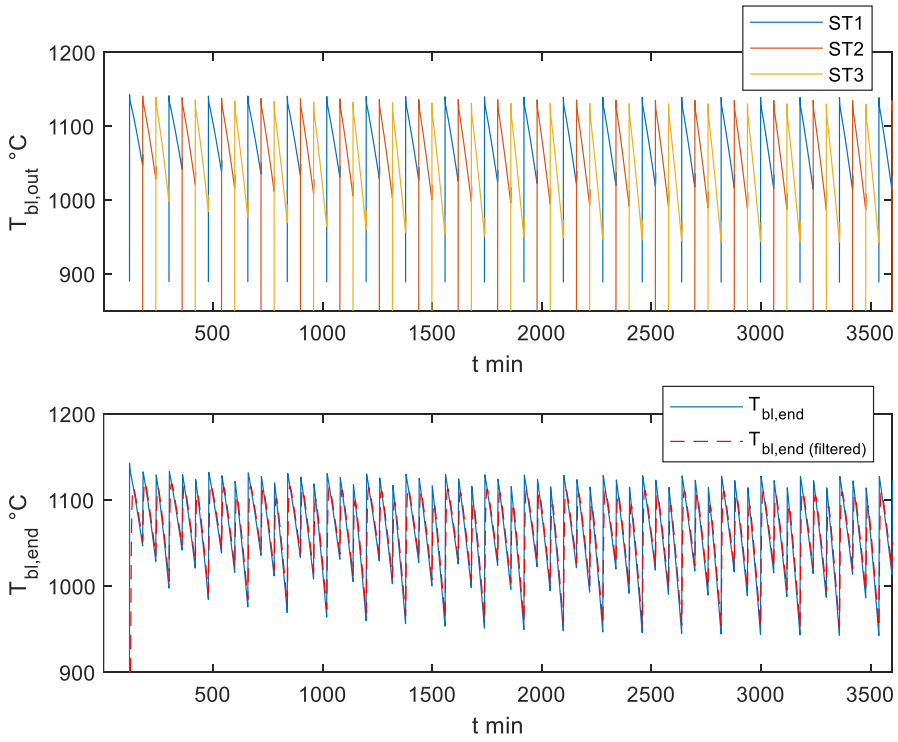

Figure 4.9 Evolution of blast temperature during the first 20 cycles for Case 2A

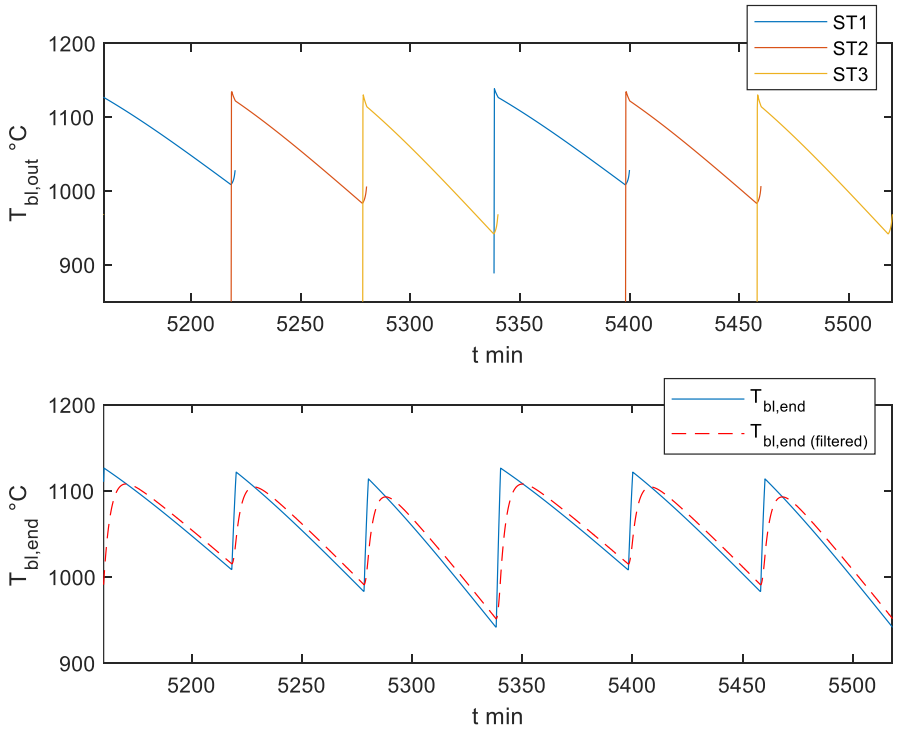

Figure 4.10 Predicted temperature of the blast after the stoves (top) and the predicted temperature of the final blast after flows mixing (bottom) at quasi-steady state for Case 2A

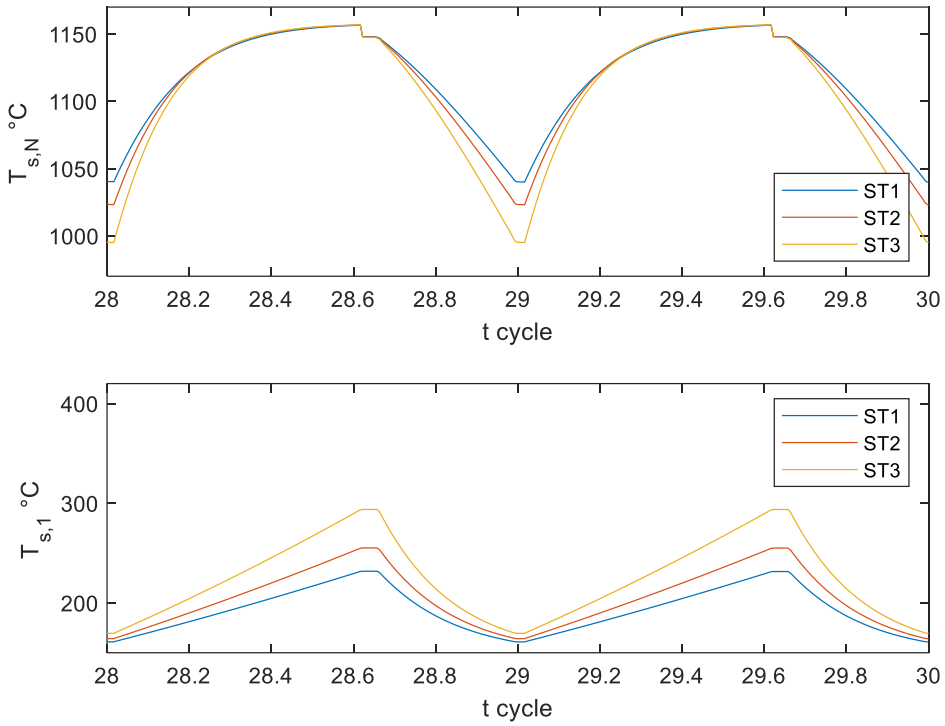

Figure 4.11 Predicted temperature of the solid at the hot end (top) and the cold end (bottom) of the checkerwork at quasi-steady state for Case 2A

Case 2B – System of Hot stoves of Different Characteristics and Different On-blast Periods

As a bypass configuration is typically implemented to control the fluctuating temperature of the outcoming hot blast, it can be expected that the final blast temperature is therefore limited to the lowest $T_{\mathrm{bl,end}}$. To elevate the overall temperature of the final hot blast, it is intuitive to adjust the length of the on-blast period of each stove based on its characteristics. This can be done by shortening the t_{blast} for the stove with lower efficiency and extending it for the stove with better efficiency, such that a stove ends its on-blast stage before its hot blast temperature drops below the desired level.

Here, the on-blast durations were chosen by trial and error and by keeping the system full cycle duration the same as in Case 2A, which is 180 minutes, yielding the values reported in the last column of Table 4.4. In this example, different t_{blast} were implemented to each stove in the system to evaluate the effect on the overall hot blast temperature. The dynamic evolution of the system is illustrated in Figure 4.12 and the predicted temperatures of the hot blast and the checkerwork at quasi-steady state are shown in Figure 4.13 and Figure 4.14. From Figure 4.13 it can be seen that the stove with better efficiency compensates the deteriorated stove and that the overall lowest $T_{\mathrm{bl,end}}$ rises by 27 °C, to 968 °C, compared to the hot-stove system in Case 2A.

The length of on-blast period for each stove should be chosen carefully so it guarantees continuous hot blast flow at the targeted temperature as well as safe operating temperature for the checkerwork. As the duration of the heating phase is determined by t_{blast}, varying this variable may give amplified effect on the $T_{\mathrm{bl,out}}$ and also on T_{s}. For a constant full cycle duration, a prolonged t_{blast} for a stove means shorter t_{heat}. Because of this, more thermal energy is discharged from the checkerwork during the on-blast period and less thermal energy is gained by the checkerwork during the on-gas period. As a result,

$T_{\mathrm{bl,out}}$ at the end of the on-blast stage becomes lower and also T_{s} decreases. The opposite effect results from a stove with a reduced t_{blast}.

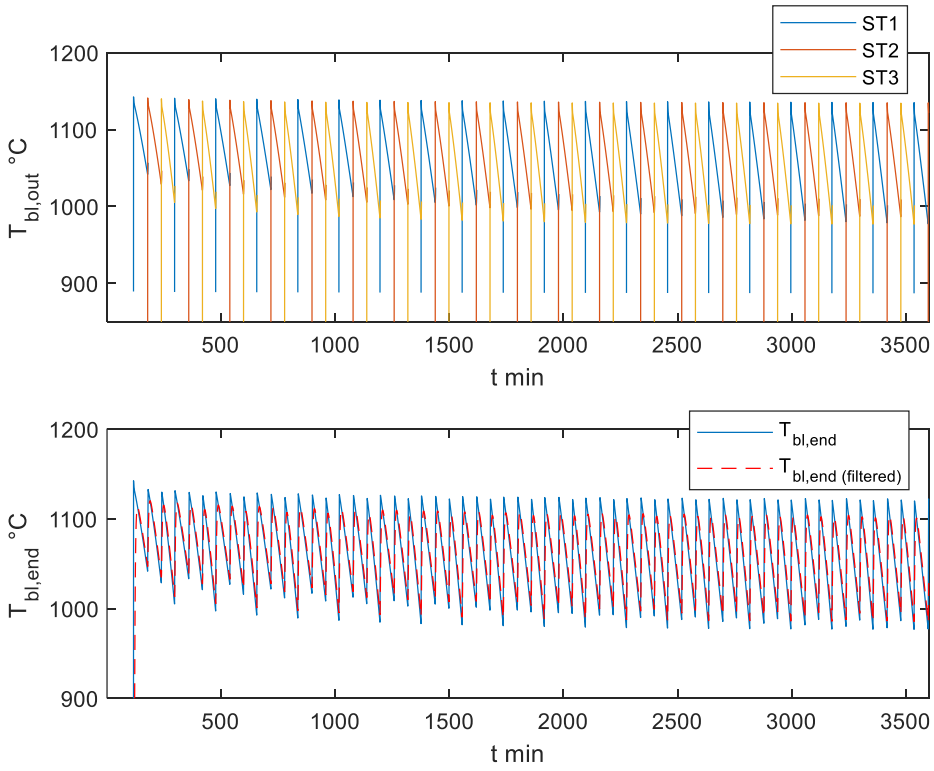

Figure 4.12 Evolution of blast temperature during the first 20 cycles for Case 2B

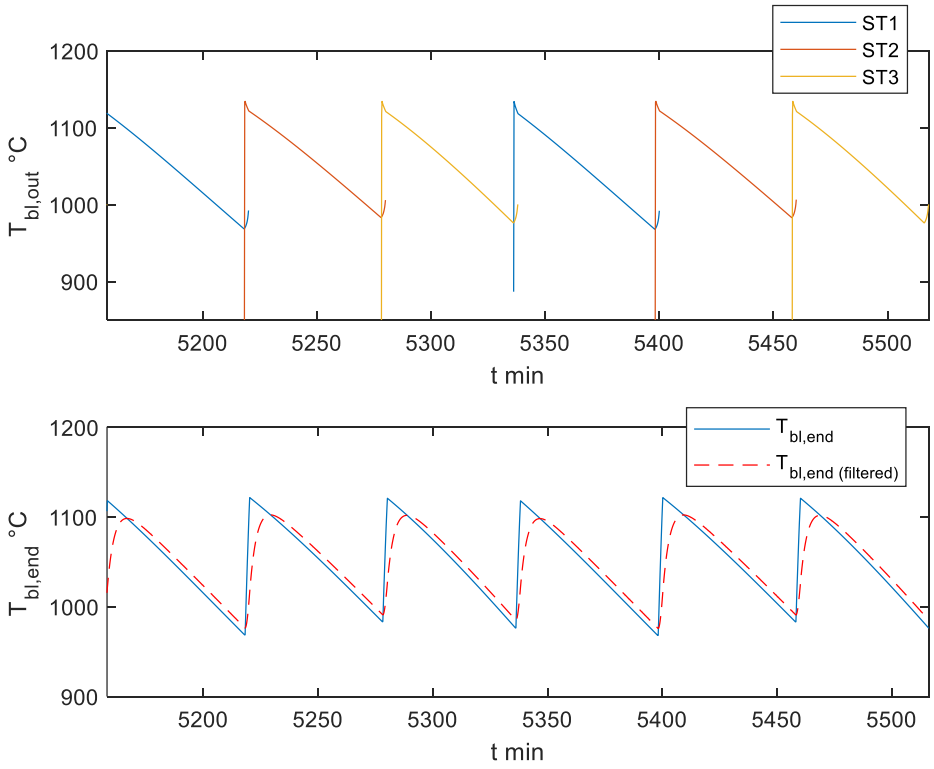

Figure 4.13 Predicted temperature of the blast after the stoves (top) and the predicted temperature of the final blast after flows mixing (bottom) at quasi-steady state for Case 2B

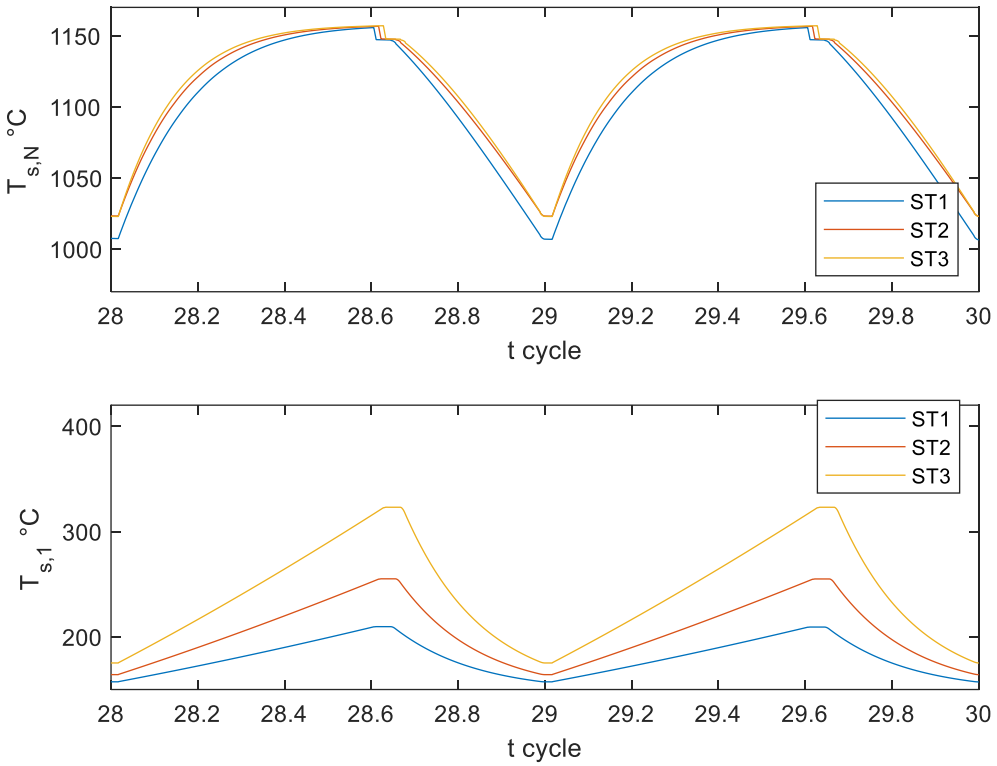

Figure 4.14 Predicted temperature of the solid at the hot end (top) and the cold end (bottom) of the checkerwork at quasi-steady state for Case 2B

Effect of the Stoves On-blast Periods on the Final Blast Temperature

When selecting t_{blast} for each stove, different combination of the stoves on-blast periods will give different overall hot-stove system performance. For a fixed full cycle duration of 180 minutes and t_{blast} of each stove ranging between 58 and 60 minutes, studied with a time step of $1/3$ min, the predicted effect on $T_{\text{bl,end}}$ is depicted in Figure 4.15. The vertical axis in the figure shows the minimum temperature of the resulting final hot blast, $T_{\text{bl,end}}^{\text{min}}$, throughout the cycles at quasi-stationary state.

Due to the characteristics of the stoves in this case, it can be expected that the feasible solutions are limited to the conditions where $t_{\text{blast},1} > t_{\text{blast},2} > t_{\text{blast},3}$. Based on the simulation results, it can be seen that shortening $t_{\text{blast},3}$ below 60 minutes to some extent can contribute to higher overall final hot blast temperature. However, for $t_{\text{blast},3} < 58$ min, a reversed trend occurs where the resulting minimum $T_{\text{bl,end}}$ starts to decrease. This happens because at too short $t_{\text{blast},3}$, the periods $t_{\text{blast},1}$ and $t_{\text{blast},2}$ become longer, and thus the temperatures of the hot blast from Stove 1 and Stove 2 become limiting.

In addition, as portrayed in Figure 4.16, too short on-blast period for Stove 3 can result in excessive thermal energy accumulation in the checkerwork, which leads to too high temperatures at the cold end of the checkerwork. $T_{\text{s,1}}^{\text{max}}$ in Figure 4.16 is the calculated highest temperature reached by the cold end of the checkerwork evaluated at quasi-stationary state operation. Therefore, for this case, it is predicted that the highest $T_{\text{bl,end}}^{\text{min}} = 975$ ℃ is achieved at $t_{\text{blast},1} = 61.67$ min and $t_{\text{blast},2} = 60.33$ min.

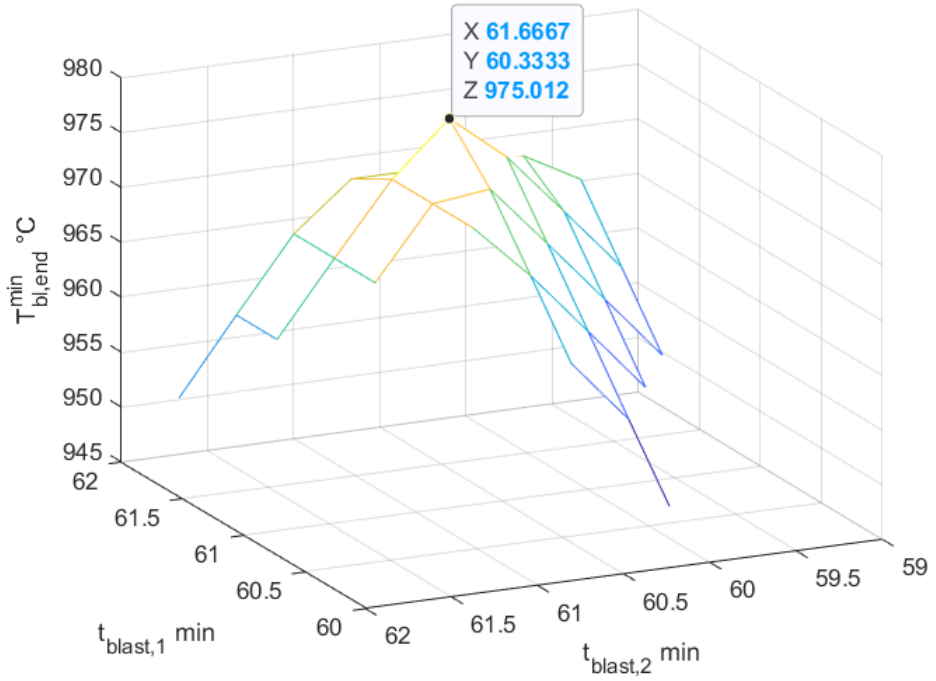

Figure 4.15 Predicted lowest temperature of the final hot blast for various combinations of the hot stoves on-blast periods in a system with total cycle length of 180 minutes (without bypass)

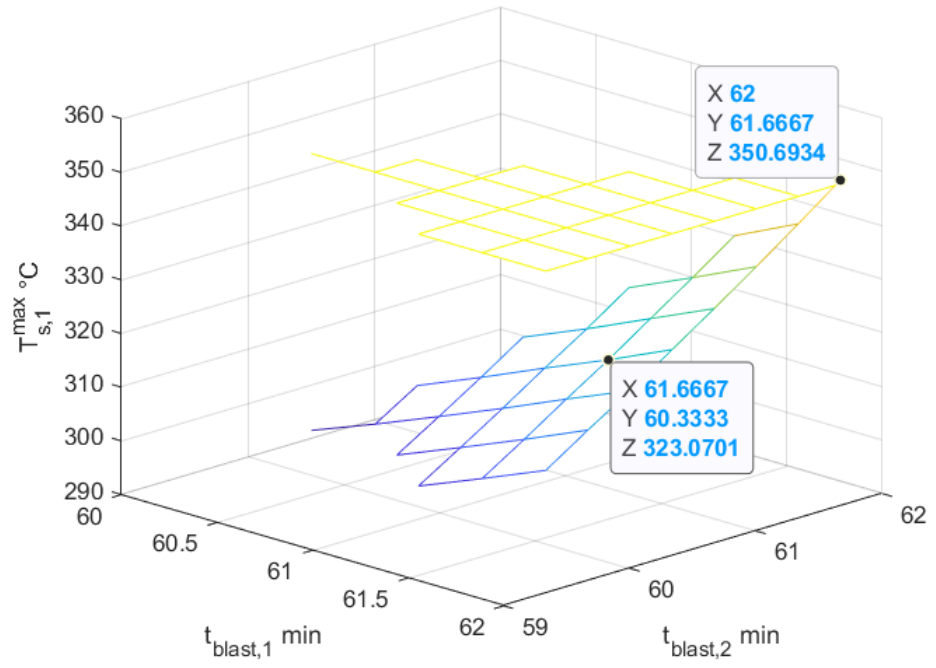

Figure 4.16 Predicted maximum temperature of the checkerwork cold end for various combinations of the hot stoves on-blast periods in a hot-stove system with total cycle length of 180 minutes (without bypass)

4.2.3 System of Hot Stoves of Different Characteristics with Bypass

In this section, systems of hot stoves of different characteristics with bypass configuration are studied. With the presence of bypass, the temperature of the final hot blast from the hot-stove system is controlled, so that it can be maintained at a desirable target temperature ($T_{\mathrm{bl,tr}}$) throughout the operation cycles. Table 4.5 lists the parameters used in the three simulated cases, Cases 3A-3C. In these cases, different duration of the system cycle, hot blast target temperature, and fuel rate were tested.

Table 4.5 Simulation parameters for Case 3

Parameter	Unit	Case 3A	Case 3B	Case 3C
η_1	-	1	1	1
η_2	-	0.8	0.8	0.8
η_3	-	0.6	0.6	0.6
$t_{\mathrm{blast},1}$	min	61.67	46	61.67
$t_{\mathrm{blast},2}$	min	60.33	45	60.33
$t_{\mathrm{blast},3}$	min	58	44	58
t_{cyc}	min	180	135	180
$T_{\mathrm{bl,tr}}$	°C	975	1000	1000
f_{fuel}	-	1	1	0.95
$x_{\mathrm{ext\ fuel}}$	-	0	0	0

Case 3A – System of hot stoves with $t_{\mathrm{cyc}} = 180$ min and $T_{\mathrm{bl,tr}} = 975$ ℃

Figure 4.17 shows the transient state of the hot-stove system during the first 20 simulated cycles. Obviously, compared to the simulated cases of the systems without bypass, the hot-stove system with bypass stabilizes to quasi-stationary state considerably faster. Although this could also be influenced by the starting temperature of the checkerwork at the initial condition, which is probably already quite close to that in the quasi-stationary state, the presence of the blast controller in the system clearly drives the system to converge to the blast temperature target.

Figure 4.18 presents the temperature of the hot blast from the stoves (upper panel) and the final blast temperature obtained after "mixing" of the former with the bypass flow (lower panel). According to the evaluation in the previous section, the hot-stove system with same operating parameters should be able to uphold a stable final hot blast temperature at a set point of about 975 °C. However, the present simulation predicted slightly different thermal behavior for this system with bypass configuration due to the different quantities of blast passed through the checkerwork – mainly during the blast transition phase, and also due to the lagging blast share controller model.

In general, the simulated $T_{\mathrm{bl,end}}$ can be maintained around the target during the on-blast period. However, at quasi-steady state it appears to be somewhat lower than the targeted temperature. This mismatch is likely due to the use of the simplified equation for temperature controller that calculates the blast share as described in Equation (21) in Chapter 3. The blast share flowing into the hot stove, $x_{\mathrm{bl,in}}(t)$, during the on-blast period is determined based on the hot blast temperature coming out from the stove at the previous time step, (t-1), which is higher than that at the current time step. In addition, some temperature spikes and falls (with a lowest $T_{\mathrm{bl,end}} = 953$ ℃) appear during the blast transition periods, since no bypass controller model is yet implemented during the blast transition stages in the simulation. With a more appropriate controller model in future studies, these issues may be resolved.

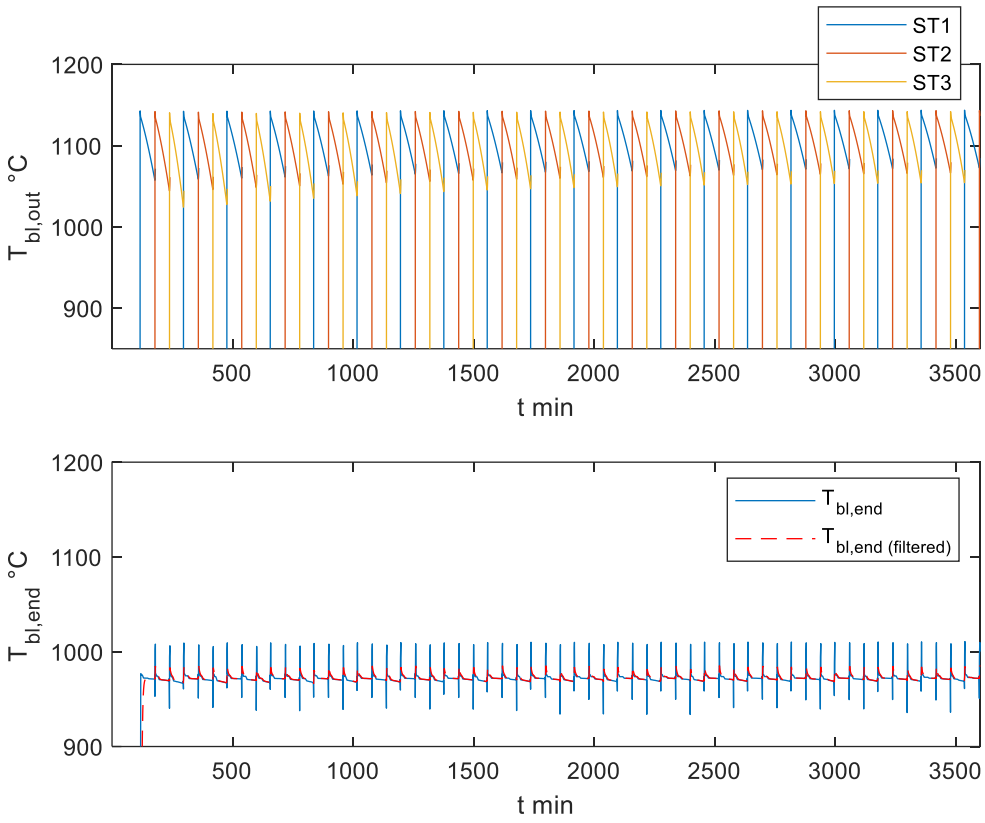

Figure 4.17 Evolution of blast temperature during the first 20 cycles for Case 3A

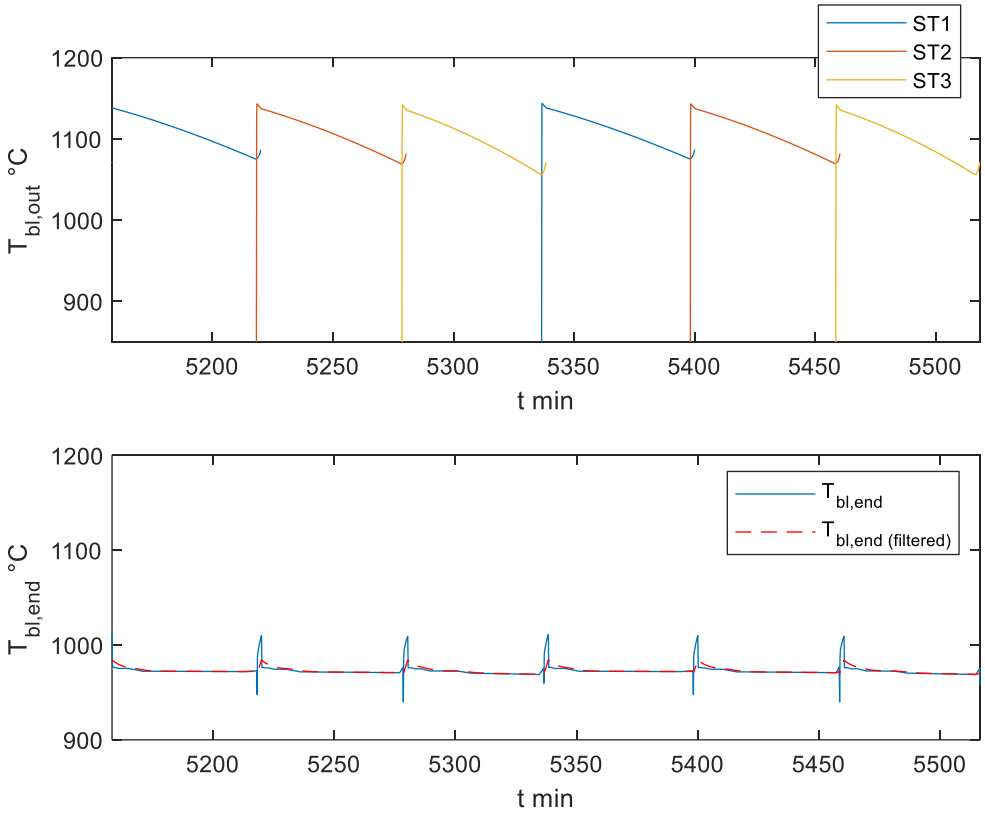

Figure 4.18 Predicted temperature of the blast after the stoves (top) and the predicted temperature of the final blast after flows mixing (bottom) at quasi-steady state for Case 3A

The blast share profile with time at quasi-steady state for Case 3A is depicted in Figure 4.19. With the bypass configuration, only a share of the cold blast passes though the hot stoves. Because of this, the blast temperature after the stoves (before mixing with bypass) is quite high, above 1050 °C, compared to that in the hot-stove system without bypass in Case 2B, where it is below 1000 °C. Moreover, this also results in even higher checkerwork temperature at the cold end of Stove 3, which exceeds the maximum limit of 350 °C (cf. bottom panel of Figure 4.20).

In hot-stove systems with bypass, while $T_{\mathrm{bl,tr}}$ is clearly determined by the requirement of the blast furnace operation, $T_{\mathrm{bl,tr}}$ also influences the dynamics of the system. The control system governs the $x_{\mathrm{bl,in}}$ so that the final blast temperature falls at the target, $T_{\mathrm{bl,tr}}$. Therefore, $T_{\mathrm{bl,tr}}$ indirectly determines the cooling rate of the stoves as well as the last hot blast temperature from the stove at the end of its on-blast period. At a higher target, a larger share of cold blast is fed into the hot stove and thus more thermal energy is drained from the stove, lowering the temperature of the checkerwork. From Figure 4.19 it can be noticed that the share of the cold blast flowing into the hot stoves at any time point in quasi-stationary state does not reach 100%. Ideally, in a well-adjusted system, the blast share starts at a level below 100% in the beginning of the on-blast phase, and then increases to 100% at the end of the on-blast period. This means that the $T_{\mathrm{bl,tr}}$ in Case 3A could have been set higher.

Considering the factors affecting the hot-stove system operation, the feasible operating conditions for the hot-stove system with bypass in the following cases were approached through several scenarios including setting a higher $T_{\mathrm{bl,tr}}$, reducing the full cycle duration, and lowering the fuel level.

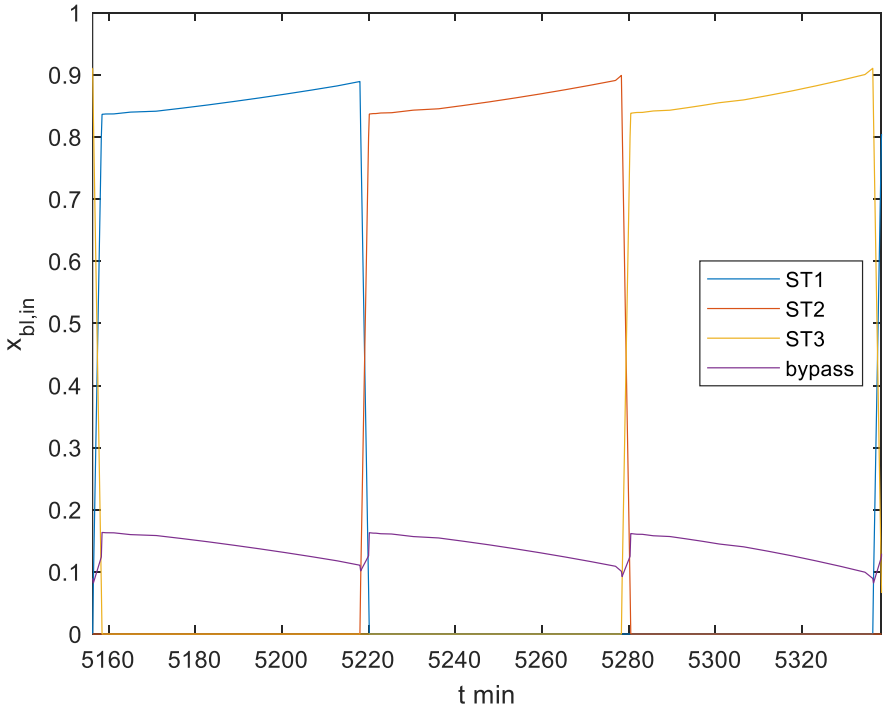

Figure 4.19 Calculated share of the cold blast passing through the hot stoves during the main blast period at quasi-steady state for Case 3A

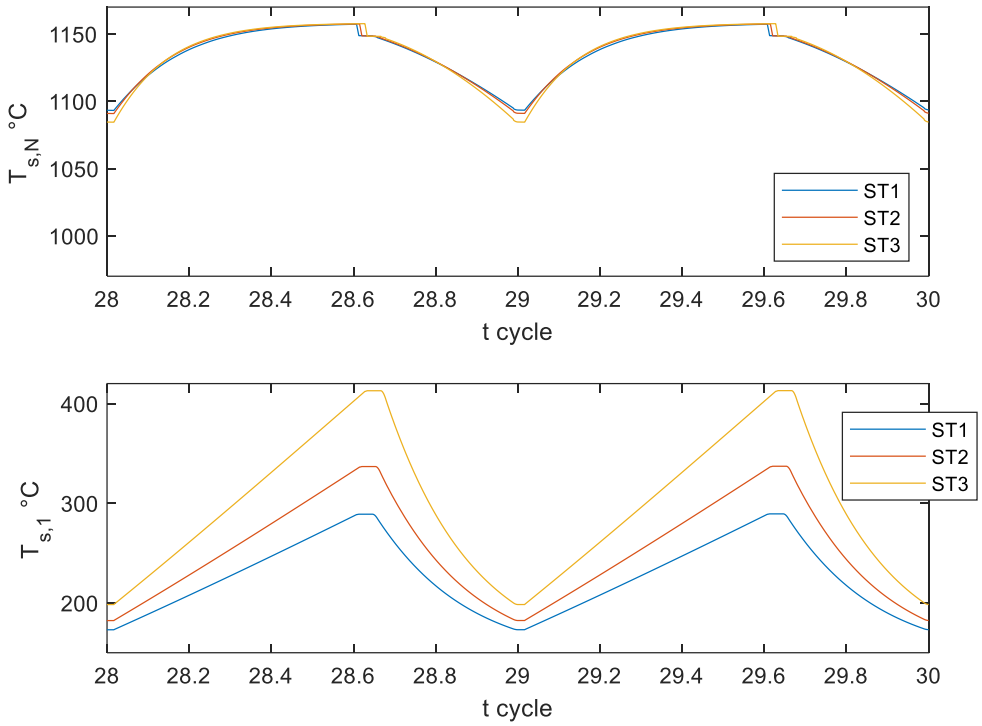

Figure 4.20 Predicted temperature of the solid at the hot end (top) and the cold end (bottom) of the checkerwork at quasi-steady state for Case 3A

Case 3B – System of hot stoves with $t_{cyc} = 135$ min and $T_{bl,tr} = 1000$ °C

Simulation results of a higher target blast temperature combined with a shorter cycle duration are presented in this example. Here, the on-blast periods for the stoves were set 46 min, 45 min, and 44 min for Stove 1, 2, and 3 respectively, which means the cycle duration is shorter compared to that in Case 3A. The dynamic evolution of the system is illustrated in Figure 4.21 and the predicted temperatures of the hot blast and the checkerwork at quasi-steady state are shown in Figure 4.22 to Figure 4.24.

From Figure 4.22 it can be seen that the predicted hot blast temperature can be stabilized at the desired temperature target. In addition, the temperature spikes and dips during the blast transitions are found to be clearly lower compared to Case 3A. It can also be observed from Figure 4.23 that with a shorter cycle duration, the blast flow share starts at a higher level initially, and then gradually increases close to one at the end of the on-blast period. One possible reason for this is that at a shorter cycle duration, the on-gas period also becomes shorter and, thus, the thermal energy level in the checkerwork at the beginning of an on-blast period is likely to be not as high as that at a longer cycle duration. Therefore, the controller regulates higher share of blast flow to pick up heat from the stove so that $T_{bl,tr}$ can be achieved after mixing the blast flow with bypass air. In addition, as expected, the checkerwork's temperature at the cold end can be kept below 350 °C due to shorter full cycle length and also higher $T_{bl,tr}$ in comparison with Case 3A (cf. bottom panel of Figure 4.24).

However, one downside of a hot-stove system with a shorter full cycle duration is that the switching stages become more frequent compared to that in a system with a longer full cycle duration. If the switching/idle times must be minimized and a long period of full cycle needs to be employed, the fuel level may need to be reduced so that the temperatures across the checkerwork can be maintained below the maximum allowable level.

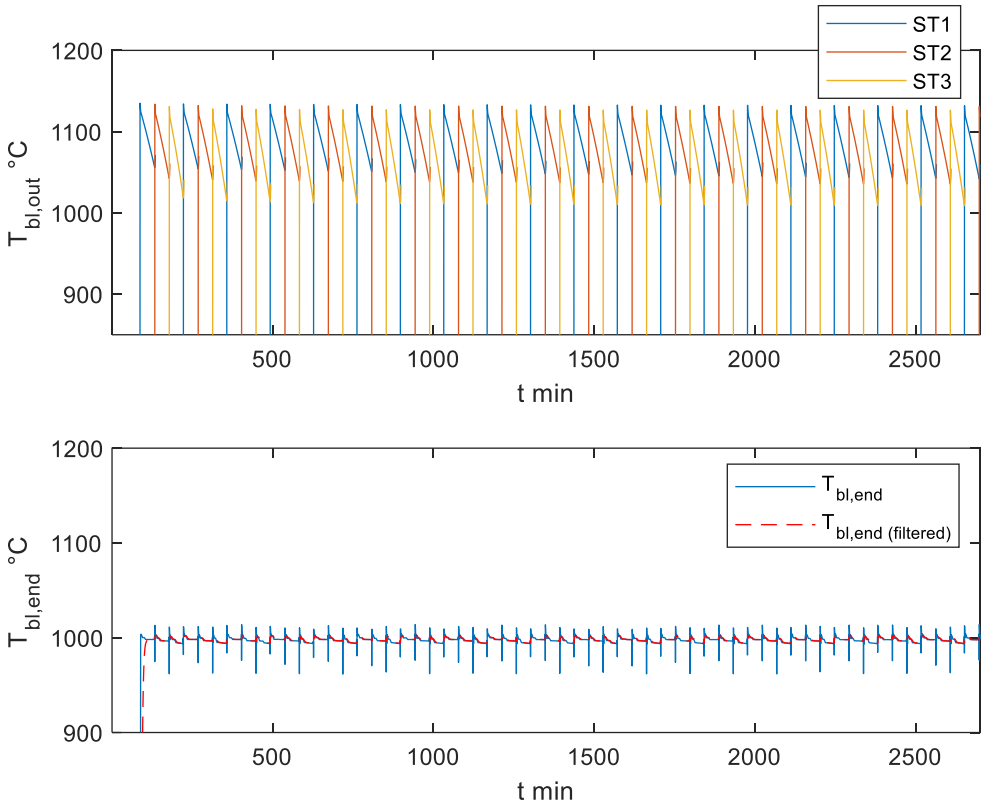

Figure 4.21 Evolution of blast temperature during the first 20 cycles for Case 3B

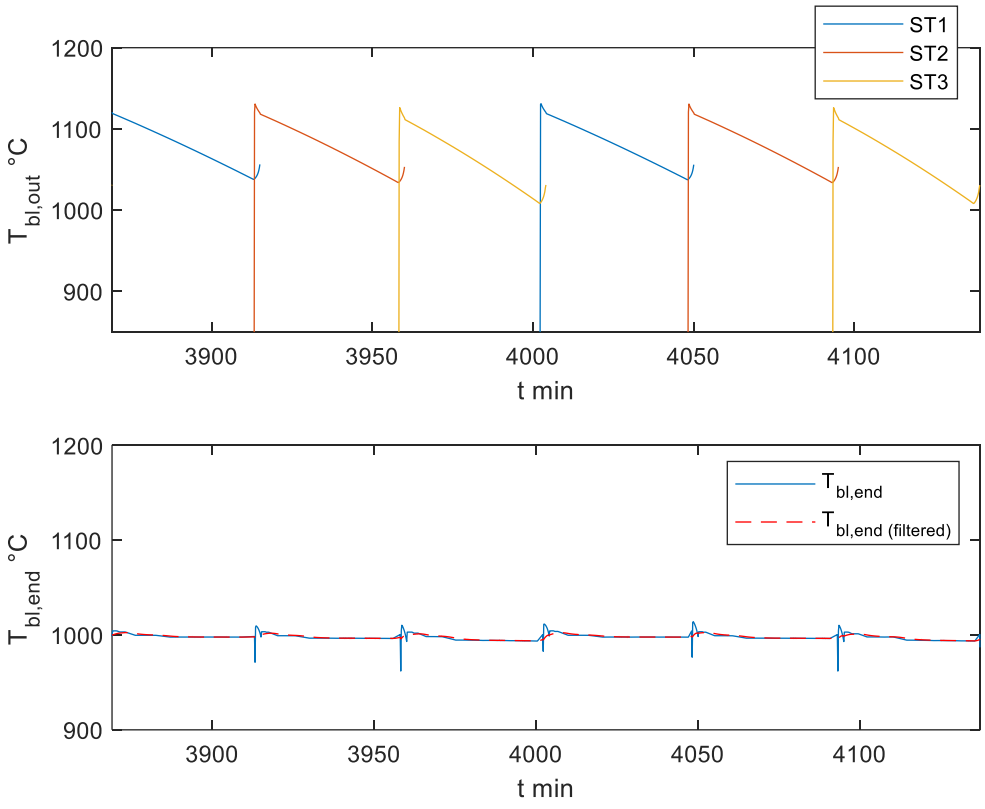

Figure 4.22 Predicted temperature of the blast after the stoves (top) and the predicted temperature of the final blast after flows mixing (bottom) at quasi-steady state for Case 3B

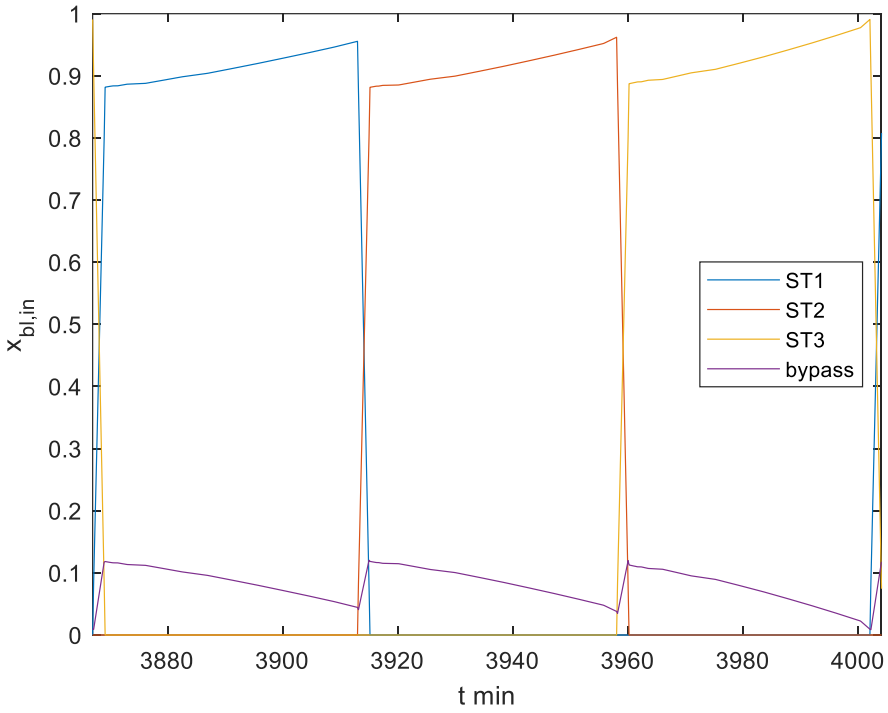

Figure 4.23 Calculated share of the cold blast passing through the hot stoves during the main blast period at quasi-steady state for Case 3B

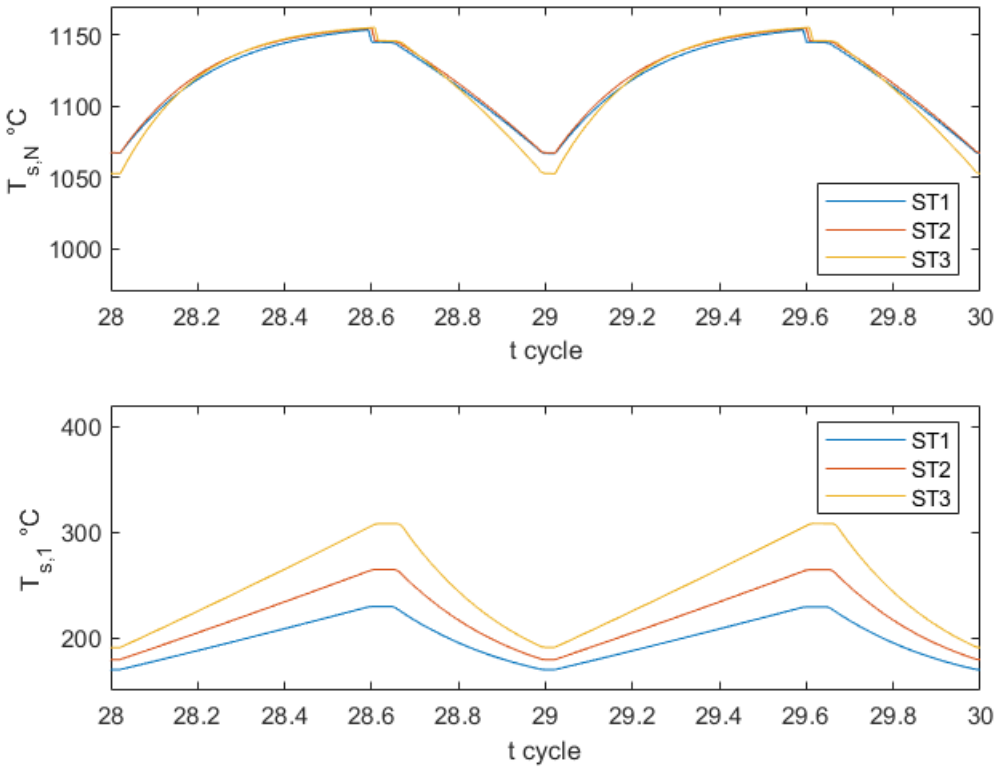

Figure 4.24 Predicted temperature of the solid at the hot end (top) and the cold end (bottom) of the checkerwork at quasi-steady state for Case 3B

Case 3C – System of hot stoves with $t_{cyc} = 180$ min, $T_{bl,tr} = 1000$ ℃, and reduced fuel level

In this example, the full cycle duration of the hot-stove system is kept at 180 minutes, with the stoves on-blast periods set to be the same as in Case 3A, but the fuel level is lowered. Simulations were run using a fuel level factor of 0.95 and also by gradually decreasing the fuel factor from 1 to 0.9 throughout the heating period. Both simulations generated practically the same results in terms of hot blast temperature and checkerwork temperature profiles.

The dynamic evolution of the system is illustrated in Figure 4.25 and the predicted temperatures of the hot blast and the checkerwork at quasi-steady state are shown in Figure 4.26 to Figure 4.28. Similar with Case 3B, the predicted blast temperature at quasi-steady state can relatively be maintained at the temperature target and the temperature deviations during the blast transition periods can be damped, as depicted in Figure 4.26. The blast flow share profile shown in Figure 4.27 is also similar with that in Case 3B (cf. Figure 4.23) in the sense that the stoves operate at a blast flow share close to one at the end of the on-blast periods. Furthermore, it is seen in the bottom panel of Figure 4.28 that the temperature of the solid at the cold end of the checkerwork can be maintained below 350 °C despite the 180 minutes long full cycle period. Based on this, one may say that with suitable operating parameters, the hot-stove system can adhere better to the blast temperature target as well as satisfy the operation constraints.

Although the operation scenario in this case seems plausible, further elevating the overall $T_{bl,end}$ is still the main goal, and this could potentially be achieved by operating at the maximum fuel level (in this study, maximum fuel level factor was assumed to be 1) or by adding external fuel with higher heating value. With this taken into consideration, a system of hot stoves with shorter full cycle length may be preferable to prevent significant depletion of $T_{bl,end}$ over the on-blast period as well as to prevent overheating of the checkerwork due to the long on-gas period.

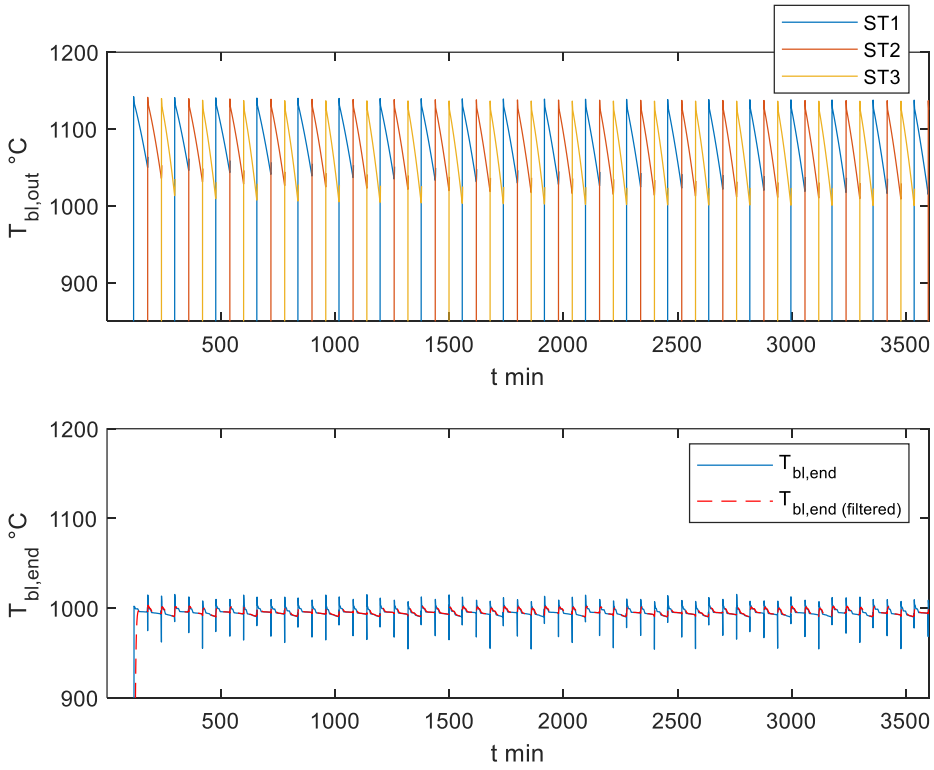

Figure 4.25 Evolution of blast temperature during the first 20 cycles for Case 3C

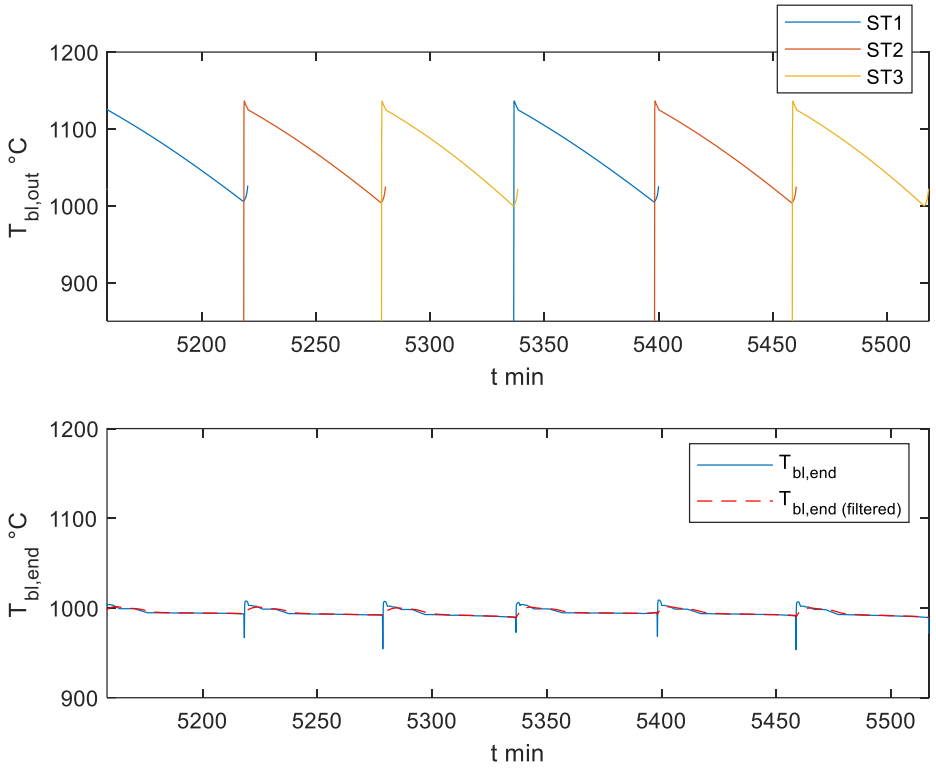

Figure 4.26 Predicted temperature of the blast after the stoves (top) and the predicted temperature of the final blast after flows mixing (bottom) at quasi-steady state for Case 3C

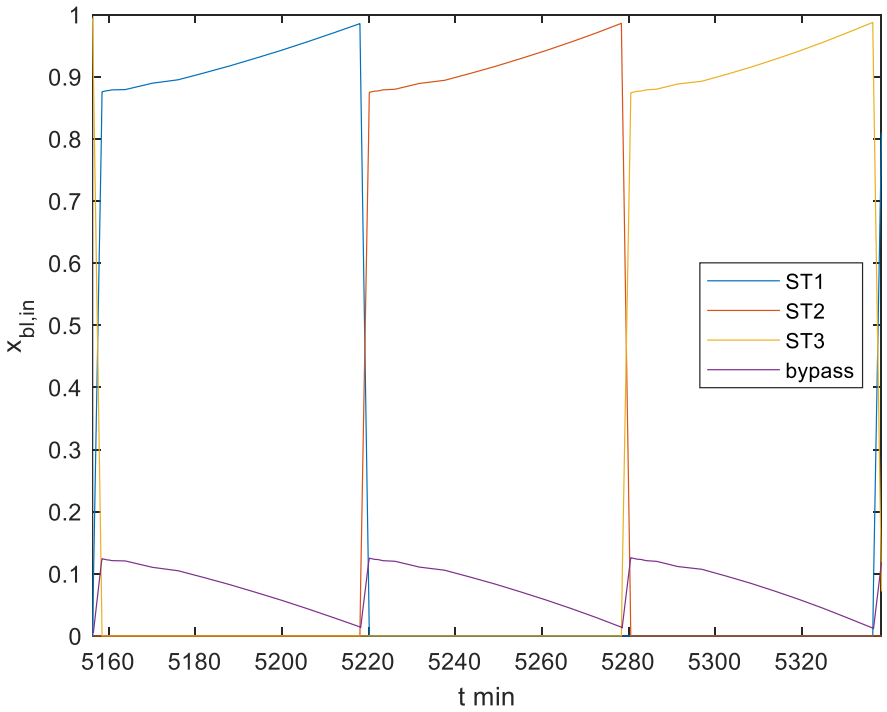

Figure 4.27 Calculated share of the cold blast passing through the hot stoves during the main blast period at quasi-steady state for Case 3C

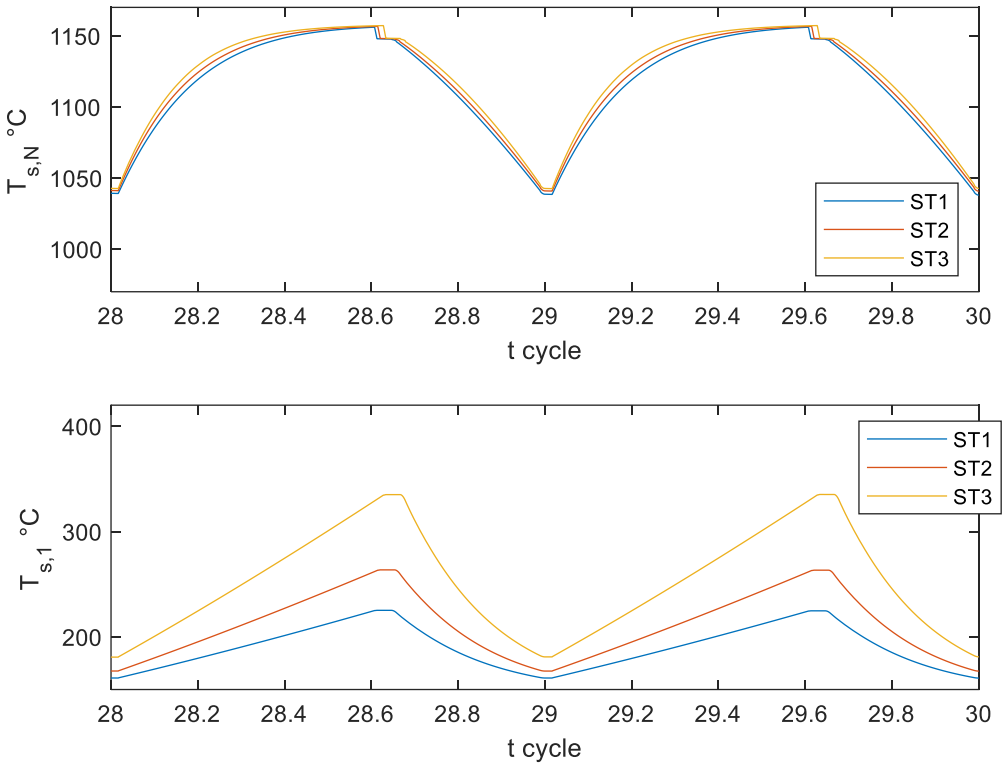

Figure 4.28 Predicted temperature of the solid at the hot end (top) and the cold end (bottom) of the checkerwork at quasi-steady state for Case 3C

Effect of the Stove On-blast Periods on the Final Blast Temperature

Similar to the hot-stove systems without bypass, different combinations of the stoves on-blast periods give different overall system performance to the hot-stove systems with bypass. Here, a system with the on-blast period for each stove ranging from 43-47 minutes and $T_{\mathrm{bl,tr}} = 1000$ ℃ is evaluated. The predicted lowest $T_{\mathrm{bl,end}}$, or $T_{\mathrm{bl,end}}^{\mathrm{min}}$, are shown in Figure 4.29. Note that here $T_{\mathrm{bl,end}}^{\mathrm{min}}$ reads the lowest temperature of the final blast, which appears to be the blast temperature dip during the blast transition periods, and $T_{\mathrm{s,1}}^{\mathrm{max}}$ is the highest temperature reached by the cold ends of the checkerworks. Both $T_{\mathrm{bl,end}}^{\mathrm{min}}$ and $T_{\mathrm{s,1}}^{\mathrm{max}}$ are evaluated at quasi-stationary state operation.

Based on the evaluation, the higher final hot blast temperatures are achieved mostly in the region where $t_{\mathrm{blast,1}} > t_{\mathrm{blast,2}} \geq t_{\mathrm{blast,3}}$ which in Figure 4.29 is the yellow region. In this favorable region, no considerable differences are observed in the final blast temperatures. Thus, because of the bypass configuration, the final blast temperatures in this region can be maintained relatively close to the target most of the time, despite the occasional temperature spikes and falls during the blast transitions. Nevertheless, the feasible solutions are limited by the checkerwork temperatures as depicted in Figure 4.30. In this case, for instance, the combination of $t_{\mathrm{blast,1}} = 45$ min and $t_{\mathrm{blast,2}} = 44.67$ min gives a fairly decent $T_{\mathrm{bl,end}}^{\mathrm{min}} \approx 962$ ℃ and $T_{\mathrm{s,1}}^{\mathrm{max}} \approx 273$ ℃. Other combinations with shorter $t_{\mathrm{blast,3}}$ can give a slight rise in $T_{\mathrm{bl,end}}$, but these may not be preferable as they come with considerably higher temperatures at the checkerworks cold ends (cf. Figure 4.30).

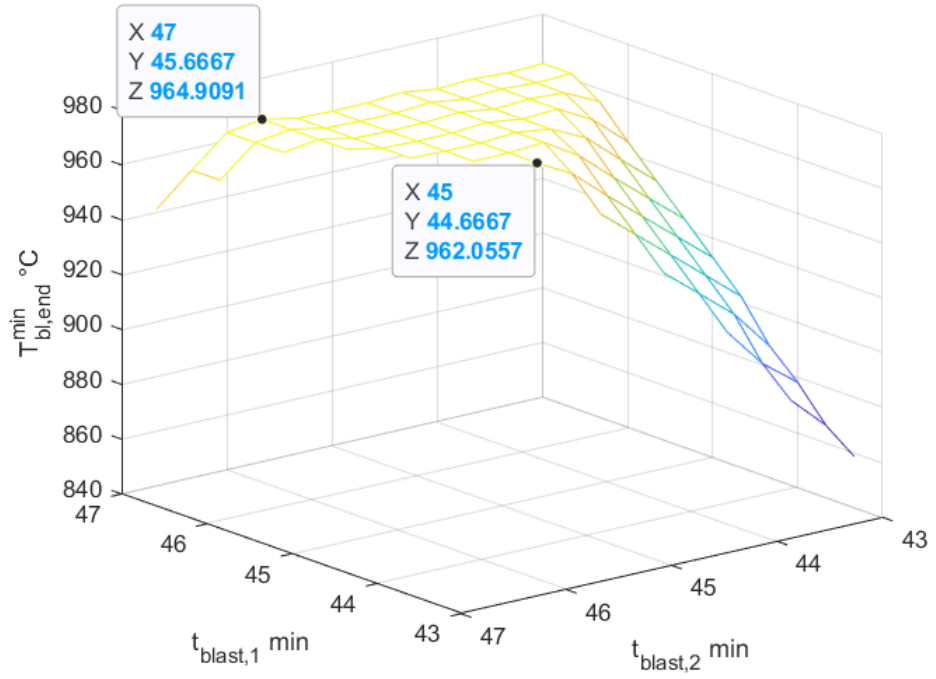

Figure 4.29 Predicted solution profile of the final hot blast lowest temperature for various combinations of hot stoves on-blast periods in a system with total cycle length of 135 minutes and blast targeted temperature of 1000 °C (with bypass)

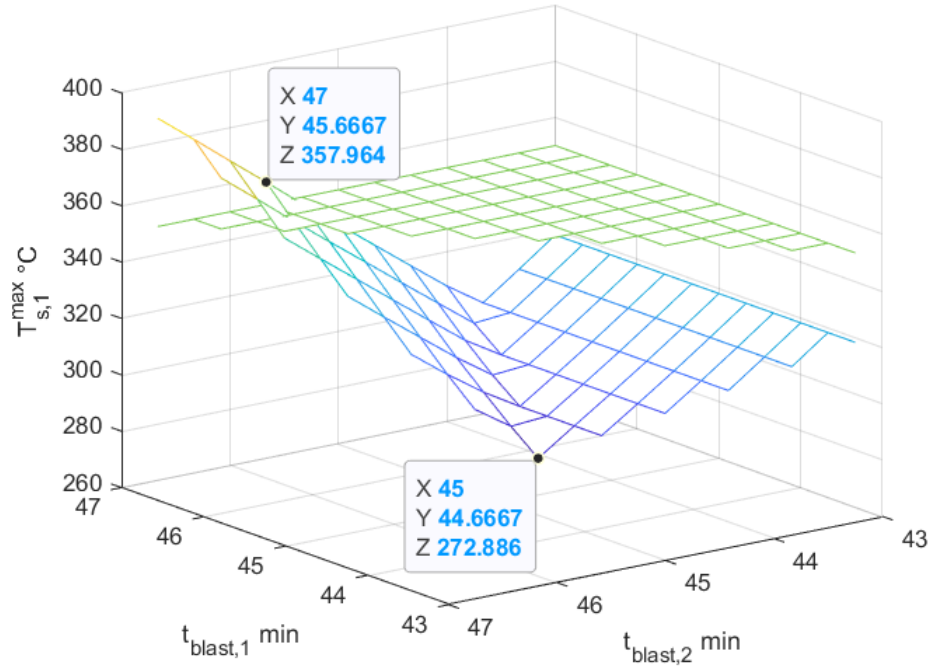

Figure 4.30 Predicted maximum temperature of solid at the cold end of the checkerwork for various combinations of hot stoves on-blast periods in a system with total cycle length of 135 minutes and blast targeted temperature of 1000 °C (with bypass)

4.2.4 Optimization Study of Hot-Stove System with Bypass

An optimization study of the hot-stove system with bypass was done through searching the local maximum of the feasible final blast temperatures $T_{\mathrm{bl,end}}$ by adjusting some contributing variables, which in this work include the duration of the on-blast period for each stove ($t_{\mathrm{blast},i}$), the final target temperature ($T_{\mathrm{bl,tr}}$) and the share of external fuel, which in this study is coke oven gas. The fuel level factor is not taken into account in this optimization study and thus assumed to be unity (maximum) in the calculation for all combinations, since the main fuel for the hot-stove system is the blast furnace top gas, the availability of which heavily depends on the operation state of the blast furnace.

While $t_{\mathrm{blast},i}$ can be considered as a variable that is bound to an individual stove, x_{COG} and $T_{\mathrm{bl,tr}}$ were applied to the entire hot-stove system. For simplification and also due to some limitations related to the compatibility of the computation code in running a fine local minimum search, in this optimization, t_{blast} for the stoves were fixed at the values found from the evaluation in the previous section, which are 45.00 min, 44.67 min, and 45.33 min for Stove 1, 2, and 3 respectively. The ranges of the other variables in this study are defined below. The composition of coke oven gas used in this study is reported in Table 4.6; the estimated heating value for it is 19 MJ/m^{3}n.

$$0 \leq x_{\mathrm{COG}} \leq 0.035$$

$$1050 \ \leq T_{\mathrm{bl,tr}} \leq 1120\ ℃$$

Table 4.6 Coke oven gas composition used in this work

Parameter	Value	Unit
$y_{\mathrm{CO,COG}}$	5.3	%
$y_{\mathrm{CO_2,COG}}$	1.8	%
$y_{\mathrm{H_2,COG}}$	58.1	%
$y_{\mathrm{N_2,COG}}$	6.4	%
$y_{\mathrm{O_2,COG}}$	0.1	%
$y_{\mathrm{CH_4,COG}}$	28.3	%

To also study how the variables influence the hot-stove system, the value of the optimum x_{COG} and $T_{\mathrm{bl,tr}}$ were identified by generating solution profiles of the minimum $T_{\mathrm{bl,end}}$, T_{s} at the checkerwork cold end, and T_{s} at the checkerwork hot end throughout the operation at quasi-steady state as depicted in Figure 4.31, Figure 4.32, and Figure 4.33. Obviously, higher x_{COG} and higher $T_{\mathrm{bl,tr}}$ result in higher $T_{\mathrm{bl,end}}$. In addition, because of the small coke oven gas addition, the calculated temperature of the combustion gas for any x_{COG} in this optimization study is still relatively low. Therefore, no variable combinations gave a predicted T_{s} at the checkerwork hot end above 1300 °C, as shown in Figure 4.33.

However, it is important to note that the resulting $T_{\mathrm{bl,end}}$ is ideally at least the same as the target, $T_{\mathrm{bl,tr}}$, or in this case, is defined to be as close as possible to it. For instance, at (a maximum) $x_{\mathrm{COG}} = 0.035$ and $T_{\mathrm{bl,tr}} = 1120\ ℃$, the lowest $T_{\mathrm{bl,end}} = 1064℃$, which is quite far lower than the targeted temperature. This may indicate that the system cannot drive up to the targeted temperature steadily and therefore this solution might not be favorable.

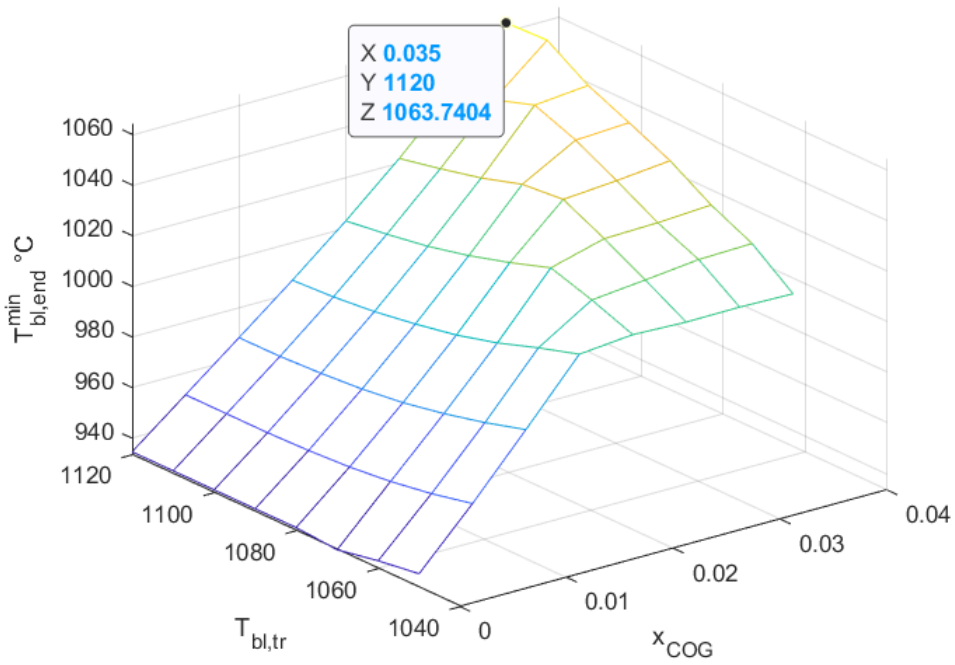

Figure 4.31 Solution profile of the final hot blast minimum temperature as a function of coke oven gas share in the fuel and the hot blast temperature set point

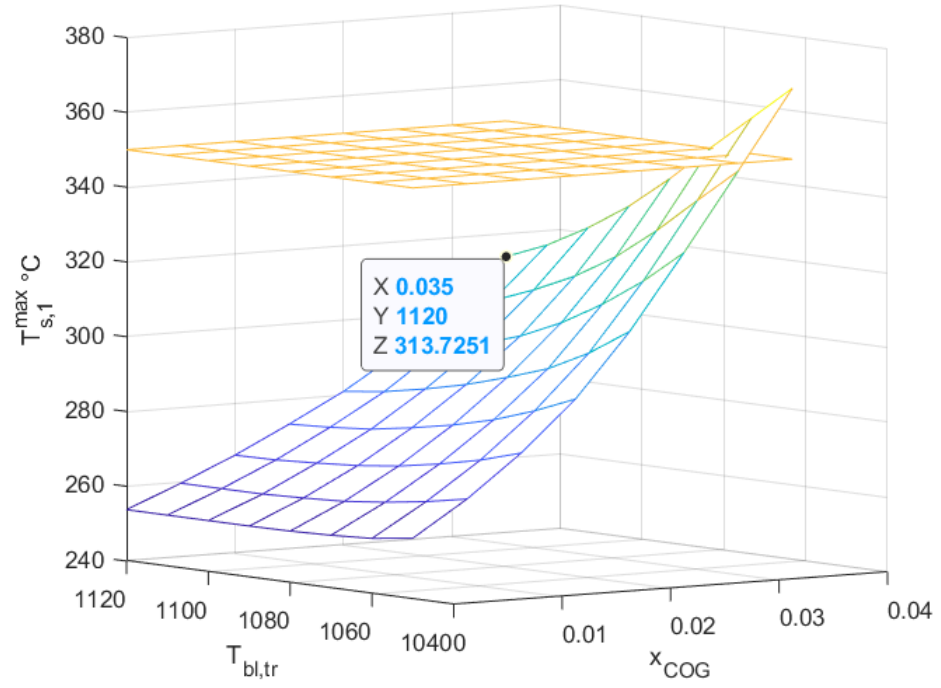

Figure 4.32 Solution profile of the checkerwork cold end maximum temperature as a function of coke oven gas share in the fuel and the hot blast temperature set point

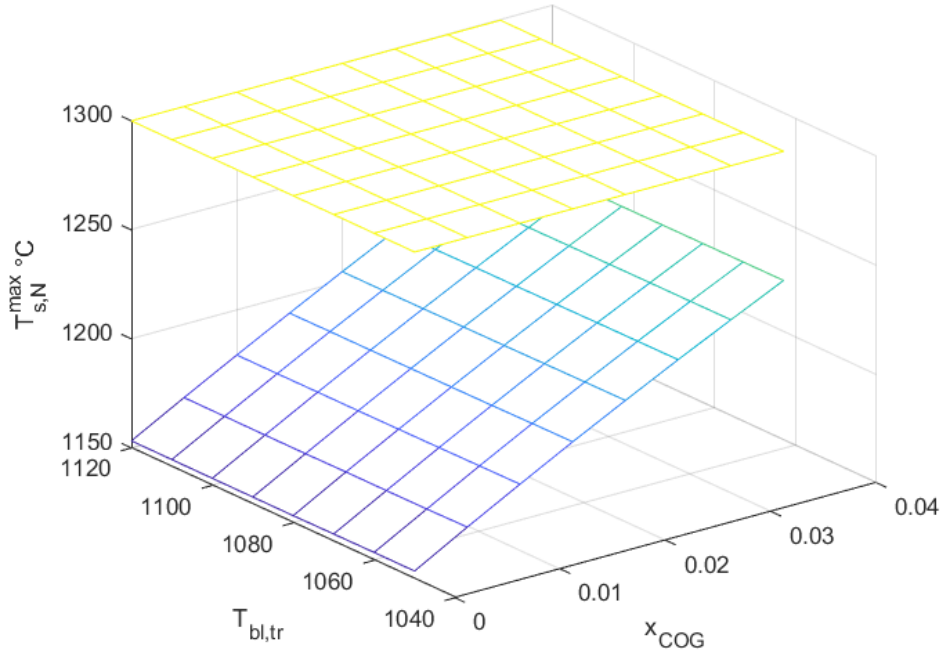

Figure 4.33 Solution profile of the checkerwork hot end maximum temperature as a function of coke oven gas share in the fuel and the hot blast temperature set point

To ensure that the system is capable to run in a relatively stable manner, another constraint was imposed, in which the deviation between $T_{\mathrm{bl,end}}$ and $T_{\mathrm{bl,tr}}$ is limited to be below 45 °C. The defined limit of the difference in this optimization study is quite big, but the temperature drops during the blast transition phase are still inevitable in this simulation setup, nonetheless. The predicted $T^{\mathrm{min}}_{\mathrm{bl,end}}$ and $T^{\mathrm{max}}_{s,1}$ of the solutions that satisfy this constraint are presented in Figure 4.34 and Figure 4.35.

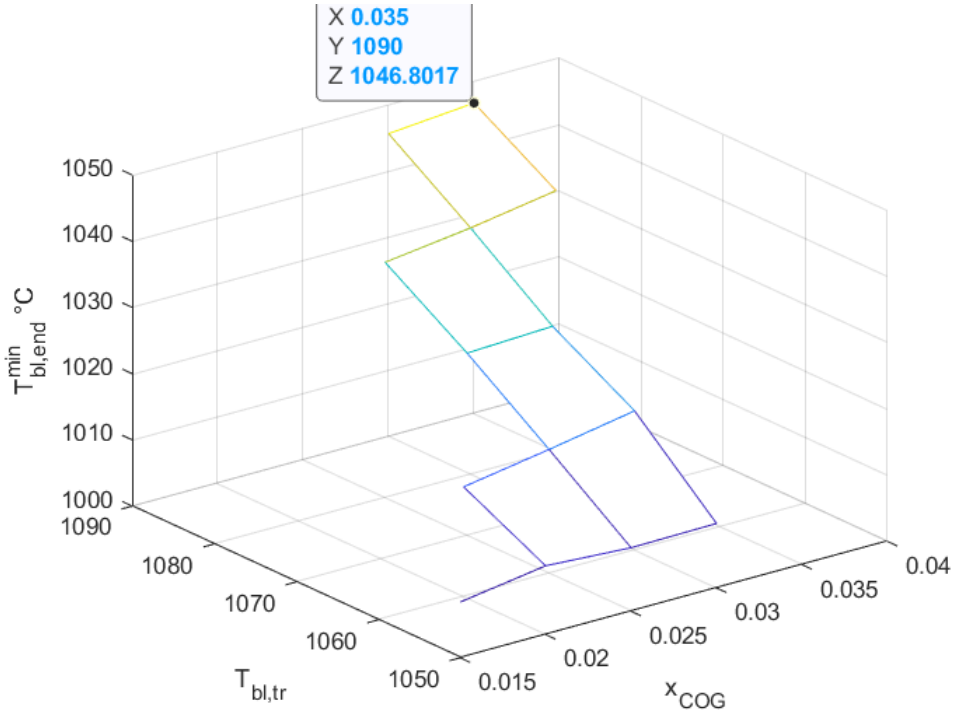

Figure 4.34 Predicted final hot blast minimum temperature based on sorted feasible solutions of the optimization study

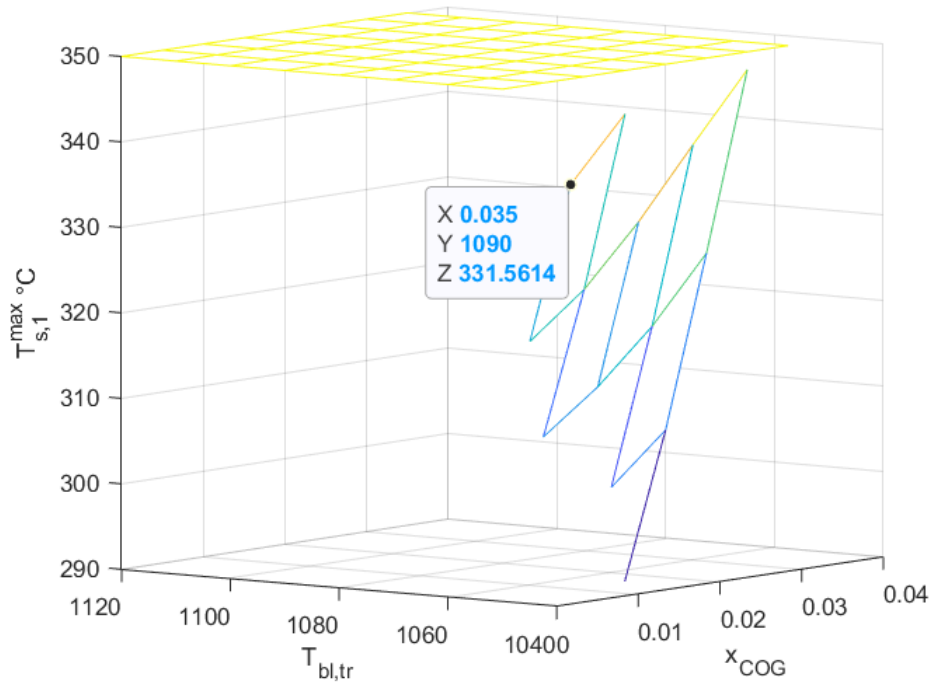

Figure 4.35 Predicted maximum temperature of the checkerwork cold end based on sorted feasible solutions of the optimization study

Based on the results obtained in this evaluation and by considering a safe operating temperature for the checkerwork, the optimum operating conditions for this problem is selected to be at $x_{\mathrm{COG}} = 0.035$ and $T_{\mathrm{bl,tr}} = 1090$ ℃. With this combination, the predicted minimum temperature of the final hot blast is 1047 °C and the maximum temperature reached at the checkerwork cold end is 332 °C. The addition of this small amount of coke oven gas rises the combustion gas temperature to 1243 °C.

5 Conclusions

A dynamic model for simulation of the operation of a hot-stove system has been developed and evaluated in this work. Several cases were investigated to examine how the hot stoves characteristics, the bypass configuration, and the system operation variables influence the behavior as well as the performance of the entire stove system. In addition, a brief optimization problem with the goal to achieve maximum blast temperature has been studied.

Based on the simulated cases of hot stoves without bypass, it was found that the lowest blast temperature rises to a certain extent alongside with longer full cycle period, since the heating duration becomes longer. In addition, in a simulated base case of a system of hot stoves with different characteristics and without bypass, the results showed that the overall final blast temperature can be elevated by almost 30 °C from the base point by only adjusting the on-blast periods for the stoves, i.e., by shortening the on-blast period of the stove with lower efficiency and extending the on-blast period of the stove with better efficiency. Due to the operation sequence, the hot stoves in the system are greatly interconnected, and a change in the on-blast duration of an individual stove can give either an amplified effect or a counterbalanced effect to the overall final blast temperature. Therefore, a solution profile of final blast temperature was generated to evaluate the optimum hot stoves on-blast periods combination.

While the blast temperature from each stove decreases throughout its on-blast stage in the system without bypass, it is possible for the final blast temperature to be maintained at a desired level in the system by mixing the hot blast with bypass blast. Due to the diversion of a share of the blast flow, it is natural for the hot stoves with bypass configuration to have the tendency in accumulating more heat, resulting in higher checkerwork cold-end temperatures. Based on the tested cases, the maximum allowable temperature at the checkerwork grid can be conformed, among other things, by operating at shorter duration of system full cycle, setting higher blast target temperature, as well as reducing the blast furnace top gas supply. As further elevating the final blast temperature is the main interest of this work, a brief optimization study was performed to search for the point at which the blast temperature target and the amount of coke oven gas used as additional fuel yields a feasibly high blast temperature while at the same time the operation constraints are satisfied. As an illustrative figure, based on the simulation results, the optimized operation of the system of hot stoves of different characteristics and with bypass configuration enables a quite considerable final blast temperature increase of above 100 °C, compared to the base case of the system without bypass nor any adjustments.

Although the simulations in this work were performed using a set of predefined parameters, the model already considers the heat transfer phenomena and the interconnection between the stoves within the system, thus giving reasonable insights of how changes in different operation parameters may affect the overall performance of the hot-stove system. In the future, these parameters can be easily adjusted to better adapt to a specific hot-stove system, which would allow for a more compatible simulation and more accurate and applicable outputs. Nevertheless, there are still some simplifications taken in this work model which can be relaxed in future work. The model in this work still assumes that the internal combustion chambers in the hot stoves are fully insulated and that they do not account for any heat transfer to the checkerworks. Additionally, the pressure losses in the gas and the blast flows are not yet considered in the heat transfer calculation nor in the optimization problem. Another option for future improvement of the model would be a refinement of the bypass controller model. In addition, the possibility to include a self-preheating phase within the stove operation sequence can also be tested.

Rigorous operation optimization and investigation of strategies to operate in special operation cases, such as two-stove operation, introduction of a stove after service period/revamping, and other dynamic states would be beneficial to study in future work. Besides, the effectiveness of high emissivity coating on the checkerwork channels surface in improving hot stove performance can also be theoretically investigated. Furthermore, since the blast furnace and the hot-stove system operate in such

interconnected and interdependent way, integrated simulation of blast furnace and hot-stove system may also be interesting to explore.

References

[1] J. Zetterholm, X. Ji, B. Sundelin, P.M. Martin, C. Wang, Dynamic modelling for the hot blast stove, Appl. Energy. 185 (2017) 2142–2150. https://doi.org/10.1016/j.apenergy.2016.02.128.

[2] H. Suopajärvi, K. Umeki, E. Mousa, A. Hedayati, H. Romar, A. Kemppainen, C. Wang, A. Phounglamcheik, S. Tuomikoski, N. Norberg, A. Andefors, M. Öhman, U. Lassi, T. Fabritius, Use of biomass in integrated steelmaking – Status quo, future needs and comparison to other low-CO2 steel production technologies, Appl. Energy. 213 (2018) 384–407. https://doi.org/10.1016/j.apenergy.2018.01.060.

[3] F. Zhang, X. Li, Z. Hu, Research on High Efficiency Energy Conversion Technology for Modern Hot Blast Stove, in: TMS 2018 Energy Technol. 2018. Miner. Met. Mater. Ser., Springer, 2018: pp. 133–152. https://doi.org/https://doi.org/10.1007/978-3-319-72362-4_12.

[4] M. Nyman, Modelling and simulation of a hot stove system to optimize energy efficiency of iron-making, Åbo Akademi, 2009.

[5] A.J. Willmott, Simulation of a thermal regenerator under conditions of variable mass flow, Int. J. Heat Mass Transf. 11 (1968) 1105–1116. https://doi.org/https://doi.org/10.1016/0017-9310(68)90028-8.

[6] P. Razelos, M.K. Benjamin, Computer model of thermal regenerators with variable mass flow rates, Int. J. Heat Mass Transf. 21 (1978) 735–744. https://doi.org/https://doi.org/10.1016/0017-9310(78)90035-2.

[7] H. Kwakernaak, P. Tijssen, R.C.W. Strijbos, Optimal operation of blast furnace stoves, Automatica. 6 (1970) 33–40. https://doi.org/10.1016/0005-1098(70)90072-5.

[8] K.R. Muske, J.W. Howse, G.A. Hansen, D.J. Cagliostro, Model-based control of a thermal regenerator. Part 1: Dynamic model, Comput. Chem. Eng. 24 (2000) 2519–2531. https://doi.org/10.1016/S0098-1354(00)00614-1.

[9] K.R. Muske, J.W. Howse, G.A. Hansen, D.J. Cagliostro, Model-based control of a thermal regenerator. Part 2: Control and estimation, Comput. Chem. Eng. 24 (2000) 2507–2517. https://doi.org/10.1016/S0098-1354(00)00613-X.

[10] SSAB, The Steel Book, 2012.

[11] Y. Kimura, K. Takatani, N. Otsu, Three-dimensional mathematical modeling and designing of hot stove, ISIJ Int. 50 (2010) 1040–1047. https://doi.org/10.2355/isijinternational.50.1040.

[12] M. Helle, H. Saxén, Simulation and Optimization of Hot Stoves in a Steel Plant, in: SCANMET V - 5th Int. Conf. Process Dev. Iron Steelmak., 2016, paper 15.

[13] SSAB-Raahe, Cowper technical drawing, n.d.

[14] B. Kjellström, J. Lindberg, G. Keikkala, Combustion and gasification in theory and practice, Luleå University of Technology, 2003.

[15] F.P. Incropera, D.P. Dewitt, T.L. Bergman, A.S. Lavine, Fundamentals of heat and mass transfer, 7th ed., John Wiley & Sons Inc., 2011.

[16] R.D. Skeel, M. Berzins, A Method for the Spatial Discretization of Parabolic Equations in One Space Variable, SIAM J. Sci. Stat. Comput. 11 (1990) 1–32. https://doi.org/10.1137/0911001.

Svensk sammanfattning

Modellering, simulering, och optimering av cowperdrift

Ett alternativ att minska energiförbrukningen vid järn- och stålproduktion är genom optimerad cowperdrift. Cowprar är regenerativa motströmsvärmeväxlare som förser masugnen med ett kontinuerligt flöde av förvärmd förbränningsluft (s.k. blästerluft) vid över 1000 °C. Det finns vanligtvis tre eller fyra cowprar per masugn. Cowperdriften är synnerligen dynamisk då den består av två växlande huvudfaser, nämligen uppvärmning (”på gas”) och nedkylning (”på bläster”). Dessutom påverkar driftparametrar och egenskaper hos en individuell cowper de andra cowprarna i systemet på grund av den starka kopplingen mellan dessa.

Det är viktigt att uppnå en hög blästertemperatur vid masugndriften då det befrämjar järnmalmsreduktionsprocessen i masugnen som i sin tur leder till ökat produktivitet. Dessutom minskar behovet av koks eller andra bränslen, vilket leder till lägre CO_2-utsläpp. En tumregel är att 10 °C högre blästerlufttemperatur minskar förbrukningen av koks i masugn med upp till 1 kg/ton råjärn. Därför är det väldigt viktigt att studera och förstå cowpersystemet om man vill förbättra och effektivera stålframställningsprocessen.

Syftet med detta diplomarbete var att bygga en modell som simulerar driften hos ett system av tre cowprar som kan ha olika egenskaper och effektivitet. Modellen används som ett verktyg för att undersöka några möjliga strategier för att uppnå optimala driftsprestanda med högre eller jämnare blästertemperatur, vilket ger lägre konsumtion av koks och andra tilläggsbränslen i masugnen.

En dynamisk modell utvecklades utifrån grundläggande energibalanser och värmeöverförings-ekvationer för gaserna (bläster och rökgaser) och murverket och implementerades därefter i MATLAB. Modellen består av partiella differentialekvationer kopplade med en uppsättning algebraiska ekvationer. Innan cowpersimuleringarna utfördes utvärderades en modell för förbränningen av masugns- och koksugnsgas för att kunna simulera tillståndet hos gasen som matas in i cowprarna och som värmer upp murverket under perioder då cowpern är ”på gas”, dvs. rökgasmängd, -temperatur och sammansättning. Noggrannheten hos modellens energibalans utvärderades även med syftet att verifiera modellens giltighet. Det visade sig att felen låg under 1% med den diskretisering i rum och tid som tillämpats, vilket ansågs acceptabelt. Dessutom gjordes med modellen en analys av temperaturfördelningen i det fasta materialet runt rökgaskanalerna som visade att den radiella temperaturen varierade marginellt (endast med några grader), varför bara en rymddimension – den vertikala – beaktades i den slutliga modellen.

Modellen utnyttjades för att studera fall där man undersökte hur cowprarnas egenskaper, förbikoppling (eng. ”by-pass”) av bläster och driftvariabler inverkar på systemets prestanda. Simuleringarna som gjordes lades upp enligt följande schema. Först simulerades ett system av cowprar med identiska (fysiska) egenskaper och blästertider, utan förbikoppling. Flera cykeltider testades och det visar sig att blästertemperaturen efter cowprarna i detta system ökade något vid längre cowpercykler. Därefter utvärderades ett liknande system men för cowprar med olika termiska egenskaper. Systemet simulerades med både identiska blästertider (såsom i basfallet) samt under varierande blästertider. Resultatet visade att den slutliga blästertemperaturen kunde höjas med ca 30 °C från baspunkten genom att justera längden på cowprarnas cykler. Justeringarna som gav bättre resultat genomfördes genom att förkorta blästertiden för en cowper med dålig prestanda samt förlänga blästertiden för en cowper med god. En förändring av blästertiden för en individuell cowper kan ge antingen en amplifierad effekt eller en motverkande effekt på den slutliga blästertemperaturen hos systemet. För att illustrera detta kopplade förlopp skapades ett diagram som visar den slutliga blästertemperaturen och med hjälp av denna grafiska representation kan man studera den optimala blästertidskonfigureringen hos cowprarna.

System med förbikoppling av bläster simulerades också och resultaten visade att det är möjligt att upprätthålla blästertemperaturen på en önskad nivå genom att blanda den uppvärmda blästerluften med ouppvärmd bläster. Cowpersystemet med förbikoppling tenderar att ackumulera mer värme i murverket som leder till en högre temperatur hos detta i den ”kalla” ändan. Denna region har vanligtvis begränsningar för hur högt temperaturen tillåts öka av konstruktionstekniska skäl, men man fann att driften kunde ske utan att begränsningarna överskreds genom att bl.a. förkorta tiden för cowpercykeln, höja blästertemperaturens börvärde och minska tillförseln av gasformigt bränsle. En kort optimeringsstudie utfördes även för att finna den högsta möjliga blästertemperaturen med beaktande av samtliga driftbegränsningar. Variablerna som manipulerades i optimeringen var blästers börvärde och mängden koksugnsgas som används som tilläggsbränsle i cowpersystemet. Optimering av systemet med olika egenskaper och med förbikoppling av bläster möjliggjorde en blästertemperaturökning på över 100 °C i jämförelse med basfallet.

Modellen som utvecklades in detta arbete har beaktat värmeöverföringsfenomen och kopplingen mellan cowprarna i systemet. Därför kan modellen ge en insikt i hur förändringar i olika driftparametrar påverkar systemets prestanda. Trots att simuleringarna genomfördes med förbestämda parametrar kan dessa parametrar enkelt justeras för att reflektera en specifik uppsättning cowprar. Emellertid har fler förenklingar gjorts i detta arbete. Modellen beaktar endast värmeöverföringen till/från murverket medan värmeflöde varken från eller till förbränningskammaren i cowpern har beaktats. Dessutom beaktas inte heller tryckförlusten för rökgas- och blästerluftsflödet i värmeöverföringsberäkningarna eller i cowperoptimeringen. En ytterligare möjlighet att förbättra simuleringarna är att finjustera regleringen av förbikopplingen av bläster i modellen. Möjligheten att inkludera en förvärmningsperiod inom cowperdriften kan också utvärderas i framtiden. En rigorös optimeringsstudie och utredning av driftsstrategier under speciella förhållande, såsom två-cowperdrift, ibruktagande av en cowper efter en underhållsperiod, och andra dynamiska tillstånd kan också vara fall som borde utforskas. Slutligen kan det vara intressant att studera en integrerad simulering av masugn och cowprarna för att få förståelse för hur de två processenheterna påverkar varandra.

Appendix – Derivation of Gas and Solid Temperature Model

The general energy balance for gas flowing through a single tube, by neglecting the effect of pressure gradient, can be written as

$$\dot{m}_{\mathrm{g}}\, c_{\mathrm{p,g}} \left[\frac{\partial T_{\mathrm{g}}}{\partial t} + \frac{\partial T_{\mathrm{g}}}{\partial z}\right] = h\, A_{\mathrm{w,i}}\, (T_{\mathrm{w,i}} - T_{\mathrm{g}})$$

or

$$\rho_{\mathrm{g}}\, \dot{V}_{\mathrm{g}}\, c_{\mathrm{p,g}} \left[\frac{\partial T_{\mathrm{g}}}{\partial t} + \frac{\partial T_{\mathrm{g}}}{\partial z}\right] = h\, \pi D_{\mathrm{h}} dz\, (T_{\mathrm{w,i}} - T_{\mathrm{g}})$$

in which the term on the left-hand side of the equation is the heat accumulation term and the term on the right-hand side is the heat flow through the inner wall.

The gas volume inside the tube is

$$V_{\mathrm{g}} = \frac{1}{4}\pi D_{\mathrm{h}}^2 dz$$

Dividing both sides of the gas energy balance equation by the gas volume, we get

$$\rho_{\mathrm{g}} c_{\mathrm{p,g}} \left[\frac{\partial T_{\mathrm{g}}}{\partial t} + v_{\mathrm{g}} \frac{\partial T_{\mathrm{g}}}{\partial z}\right] = \frac{4h}{D_{\mathrm{h}}} (T_{\mathrm{w,i}} - T_{\mathrm{g}})$$

The general energy balance for the solid over a single tube, by neglecting the conduction in the radial direction, is described by

$$m_{\mathrm{s}}\, c_{\mathrm{p,s}}\, \frac{\partial T_{\mathrm{s}}}{\partial t} - V_{\mathrm{s}}\, k_{\mathrm{s}} \frac{\partial^2 T_{\mathrm{s}}}{\partial z^2} = h\, A_{\mathrm{w,i}} \left(T_{\mathrm{g}} - T_{\mathrm{w,i}}\right) - h_{\mathrm{loss}}\, A_{\mathrm{w,o}}\, (T_{w,o} - T_{\infty})$$

or

$$\rho_{\mathrm{s}}\, V_{\mathrm{s}}\, c_{\mathrm{p,s}}\, \frac{\partial T_{\mathrm{s}}}{\partial t} - V_{\mathrm{s}}\, k_{\mathrm{s}} \frac{\partial^2 T_{\mathrm{s}}}{\partial z^2} = h\, 2\pi r_i dz \left(T_{\mathrm{g}} - T_{\mathrm{w,i}}\right) - h_{loss}\, 2\pi r_o dz\, (T_{w,o} - T_{\infty})$$

in which the first and the second term on the left-hand side are the heat storing term and the axial conductive heat flow respectively, and the terms on the right-hand side are the heat flows through the inner and the outer wall of the solid.

The volume of the solid tube is

$$V_{\mathrm{s}} = \pi(r_o^2 - r_i^2)dz$$

Dividing both sides of the solid energy balance equation by tube volume and assuming that the heat loss is proportional to temperature of the solid at the outer wall, we get

$$\rho_{\mathrm{s}} c_{\mathrm{p,s}} \frac{\partial T_{\mathrm{s}}}{\partial t} - k_{\mathrm{s}} \frac{\partial^2 T_{\mathrm{s}}}{\partial z^2} = \frac{2h}{r_{\mathrm{i}}(r_{\mathrm{o}}^2/r_i^2 - 1)}(T_{\mathrm{g}} - T_{\mathrm{w,i}}) - \frac{2h_{\mathrm{loss}}}{r_{\mathrm{o}}(1 - r_{\mathrm{i}}^2/r_{\mathrm{o}}^2)} T_{\mathrm{w,o}}$$

Since, in this work, the temperatures of the solid in radial direction are lumped, the temperature of the solid in the radial direction is assumed to be uniform at an average level, $T_{\mathrm{w,i}} = T_{\mathrm{w,o}} = T_s$.

Thus, the final model of the system energy balance is written below.

Gas:

$$\rho_{\mathrm{g}} c_{\mathrm{p,g}} \left[\frac{\partial T_{\mathrm{g}}}{\partial t} + v_{\mathrm{g}} \frac{\partial T_{\mathrm{g}}}{\partial z} \right] = \frac{4h}{D_{\mathrm{h}}} (T_{\mathrm{s}} - T_{\mathrm{g}})$$

Solid:

$$\rho_{\mathrm{s}} c_{\mathrm{p,s}} \frac{\partial T_{\mathrm{s}}}{\partial t} - k_{\mathrm{s}} \frac{\partial^2 T_{\mathrm{s}}}{\partial z^2} = \frac{2h}{r_{\mathrm{i}}(r_{\mathrm{o}}^2/r_i^2 - 1)}(T_{\mathrm{g}} - T_{\mathrm{s}}) - \frac{2h_{\mathrm{loss}}}{r_{\mathrm{o}}(1 - r_{\mathrm{i}}^2/r_{\mathrm{o}}^2)} T_{\mathrm{s}}$$